D-MEM
PhD-UNIMI

Doctorate program
Milan
EXPERIMENTAL
MEDICINE

Università degli Studi di Milano

PhD Course in
Experimental Medicine

CYCLE XXXVII
Department of Medical Biotechnology and Translational Medicine

PhD thesis

Investigating the role of defective cell to cell communication mechanisms in Rett syndrome pathogenesis

Candidate: **Martina Breccia** (R13379)

Tutor: Prof. Angelisa Frasca

Supervisor: Prof. Nicoletta Landsberger

Director: Prof. Nicoletta Landsberger

Academic Year 2023-2024

Table of contents

Disclosure for research integrity *5*

Abbreviations *6*

Abstract *8*

1. Introduction *10*

1.1 Rett syndrome clinical features **10**

1.2 MECP2: the genetic driver of Rett syndrome **13**

1.3 Genotype – phenotype correlation **16**

1.4 Therapeutic strategies **18**

1.5 Neurobiology of RTT **19**

1.6 Astrocytes role in RTT pathogenesis **23**

2. Aim of the thesis *30*

3. Materials and methods *32*

3.1 Animals **32**

3.1.1 Animal care and genetically modified mouse lines 32

3.1.2 Genotyping 33

3.2 Primary cultures **36**

3.2.1 Primary cultures of cortical neurons 36

3.2.2 Primary cultures of cortical astrocytes 37

3.2.3 Astrocyte-neuron co-cultures 37

3.2.4 Collection of astrocyte conditioned medium (ACM) or co-culture conditioned medium (CCM) 38

3.3 MACS sorting **39**

3.4 Treatments on cell culture **40**

3.4.1 Treatment of neurons with ACM/CCM 40

3.4.2 Treatment of neurons with recombinant IL-6 40

3.4.3 Treatment of co-cultures with the neutralizing anti-IL6 antibody 40

3.4.4 Trofinetide treatment on astrocytes 41

3.4.5 Cholesterol supplementation 41

3.5 Immunofluorescence 41
3.5.1 Immunofluorescence for neuronal morphology and synaptic puncta analysis 41
3.5.2 Immunofluorescence for astrocyte marker GFAP 42
3.6 Microscopy and image analysis 44
3.6.1 Total dendritic length 44
3.6.2 Synaptic puncta on neuronal cultures 44
3.7 Gene expression analysis 45
3.7.1 RNA extraction 45
3.7.2 RNA quantification and integrity assessment 45
3.7.3 Quantitative Reverse Transcription PCR 46
3.8 Protein extraction and western blotting 47
3.8.1 Protein extraction and quantification 47
3.8.2 Western blot 48
3.9 Cytokines quantification 50
3.10 ELISA assay for IL-6 50
3.11 MTT assay 51
3.12 Statistical analysis 51
4. Results 52
4.1 Preliminary data 52
4.1.1 Factors released by *Mecp2* knock-out (KO) astrocytes are detrimental for synapse development and maintenance 52
4.1.2 Transcriptional analysis in neurons confirms the negative impact of Mecp2 KO astrocytes on synaptic phenotype, unveiling the involvement of inflammatory molecules. 56
4.2 *Mecp2* KO astrocytes affect synaptogenesis by Interleukin-6 (IL-6) dependent mechanisms 58
4.2.1 *Mecp2* KO astrocytes induce the expression of inflammatory-related factors in WT neurons 58
4.2.3 *Mecp2* KO astrocytes secrete increased levels of IL-6 only in the presence of WT neurons 61

4.2.4 Secreted IL-6 contributes to the impairment of synaptic phenotype in WT neurons 64

4.3 IL-6 expression shows a trend toward an increase in the whole cortex of symptomatic HET mice 67

4.4 Alterations in cholesterol pathway in *Mecp2* KO astrocytes affect synaptic phenotype 70

4.4.1 Cholesterol biosynthesis and transport are impaired in *Mecp2* KO astrocytes 70

4.4.2 Trofinetide treatment of *Mecp2* KO astrocytes ameliorates defective expression of cholesterol-related genes 72

5. Discussion 78

***5.1 Mecp2* KO astrocytes affect synaptogenesis by Interleukin-6 dependent mechanisms. 78**

5.2 Deregulation of cholesterol pathway in Mecp2 KO astrocytes contributes to synaptic defects. 83

5.3 Conclusion 87

Aknowledgments 88

Bibliography 89

List of figures and tables 110

Appendix 112

Dissemination of the results 126

Disclosure for research integrity

This research was conducted following the European Code of Conduct for Research Integrity, in respect of the values of reliability, rigor, honesty, respect and transparency. Care was taken to ensure the accuracy and precision of the data, the integrity of the methods used, and the thoroughness of the analysis. All sources of information have been properly cited, and any limitations of the research are openly acknowledged. Furthermore, all individuals who contributed to or participated in the research process have been recognized for their contributions.

Abbreviations

- ACM: astrocyte conditioned medium
- AVV: Adeno-associated virus
- BBB: Blood brain barrier
- BDNF: Brain-derived neurotrophic factor
- CCM: Co-culture conditioned medium
- CDKL5: Cyclin-dependent kinase-like 5
- CNS Central nervous system
- CREB1: cyclic AMP-responsive element binding protein CTD C-terminal domain
- CTD: C-terminal domain
- CRISPR-Cas9: clustered regularly interspaced short palindromic repeats - caspase 9
- CXCL12: C-X-C Motif Chemokine Ligand 12
- DEG: Differentially expressed gene
- DIV: Day *in vitro*
- E/I: Excitatory/inhibitory
- ELISA: Enzyme-linked immunosorbent assay
- FOXG1: Forkhead box protein G1
- GO: Gene ontology
- GPE: Glutamate-Proline-Glycine active tripeptide
- ID: Intervening domain
- IGF: Insulin-like growth factor
- IL-1β: Interleukin-1 beta
- IL-6: Interleukin-6
- HDAC: Histone deacetylase
- HET: Heterozygous
- ID: Intervening domain
- KI: knock-in
- KO: knock-out
- MBD: Methyl-CpG-binding domain
- MDS: MeCP2 duplication syndrome

- MECP2: Methyl-CpG-binding protein
- MRI: Magnetic resonance imaging
- NCoR-SMRT: Nuclear receptor Co-Repressor and the Silencing Mediator of Retinoic acid and Thyroid hormone receptor NID NCoR/SMRT Interaction Domain
- NF-kB: Nuclear factor kappa-light-chain-enhancer of activated B cells
- NLS: Nuclear localization signal
- NPCs: Neuronal precursor cells
- Nsdhl: NAD(P) dependent steroid dehydrogenase-like
- NTD: N-terminal domain
- p-adj: Adjusted p-value
- PCA: Principal Component Analysis
- qRT-PCR: Quantitative reverse transcription polymerase chain reaction
- RNASeq: RNA sequencing
- RTT: Rett syndrome
- SEM: Standard error mean
- STAT3: Signal transducer and activator of transcription 3
- TCA cycle: Tricarboxylic acid cycle
- TNF α: Tumor necrosis factor alfa
- WT: Wild type
- XCI: X chromosome inactivation

Abstract

Rett syndrome (RTT) is a devastating neurodevelopmental disorder representing the main cause of severe intellectual disability in girls worldwide. Over 95% of individuals suffering from a classic form of RTT carry sporadic mutations in the X-linked *MECP2* gene, encoding for the methyl-GpC-binding protein 2 (MeCP2), responsible for the regulation of the expression of thousands of genes. RTT is characterized by defects in neuronal morphology, activity and synaptic transmission, which are in part caused by the insufficient support from astrocytes. Indeed, astrocytes in RTT not only exhibit alterations in their morphology, metabolism and calcium signaling, but they also fail to adequately sustain neuronal growth and activity. Although understanding the causative mechanisms could guide the development of novel and effective therapeutic strategies, they remain largely unknown to date. This study explores the impact of *Mecp2* knock-out (KO) astrocytes on synapses, mainly focusing on the paracrine signals, exploiting two different *in vitro* culture systems. On one hand, we treated neurons with astrocyte conditioned medium (ACM) obtained from wild type (WT) or *Mecp2* KO astrocytes. On the other hand, we used a co-culture system between neurons and astrocytes, in which the latter are cultured on transwell inserts preventing the direct contact with neurons while allowing the exchange of secreted molecules. In both the cases, we observed that *Mecp2* KO astrocytes severely compromise synaptogenesis and synaptic maintenance, suggesting that they either release synaptotoxic molecules or fail to secrete necessary synaptogenic factors.

A transcriptomic study revealed that molecules secreted by *Mecp2* KO astrocytes induce an abnormal inflammatory response in neurons, and coherently we found an increase of Interleukin-6 (IL-6) levels in the medium of the co-culture. The excessive amount of IL-6 was proven to be a critical mediator of synaptic defects as its blockade with a specific neutralizing antibody significantly recovered the synaptic phenotype. However, the persistence of post-synaptic defects implies the involvement of other factors. Thus, in addition to IL-6, our investigation extended to cholesterol, a well-known synaptogenic factor, mainly provided by astrocytes in mature brain. Interestingly, *Mecp2* KO astrocytes show the downregulation of many genes involved in cholesterol synthesis and transport. Interestingly, the treatment of *Mecp2* KO astrocytes with Trofinetide, the only FDA-approved drug for RTT, rescued the expression of some of the downregulated genes, suggesting that part of the beneficial

effects elicited by this drug might be due to the modulation of cholesterol metabolism. Furthermore, cholesterol supplementation improved synaptic deficits in neurons treated with KO ACM, and similar benefits were observed in neurons obtained from heterozygous *Mecp2*$^{+/-}$ female mice.

In conclusion, this study reveals that the overproduction of IL-6 and dysregulation of cholesterol metabolism in *Mecp2* KO astrocytes have detrimental effects on synaptic health, offering novel potential therapeutic targets for RTT. These findings support the hypothesis that insufficient release of synaptogenic factors by astrocytes, combined with the release of synaptotoxic factors, contributes to pre- and post-synaptic impairments characterizing the pathology.

1. Introduction

1.1 Rett syndrome clinical features

Rett syndrome (RTT, OMIM identifier #312750) is a severe and progressive neurodevelopmental disorder representing a major cause of intellectual disability in girls worldwide, with an incidence of 1 in 10.000 live births (1). In 1966, the Austrian pediatrician Andreas Rett depicted for the first time some anomalous behaviors in 22 young female patients manifesting the presence of stereotypical hand movements as main common symptom (2). Girls also showed an impairment of motor and cognitive skills, together with breathing and gait abnormalities. Given that the work of Dr. Rett was written in German language and considering the low incidence of the pathology, the disease truly entered in the medical consciousness after about 20 years, when Bengt Hagberg, a Swedish pediatric neurologist, observed the same symptoms in some of his young female patients. In 1983, together with other physicians, he published a paper collecting the clinical descriptions of 35 girls from Sweden, France and Portugal, establishing the existence of a unique developmental disorder named Rett syndrome, in honor of its pioneering researcher (3). After the first RTT meeting, held in Vienna in 1984, neurologists tried to systematically describe disease progression (4,5). According to symptoms manifestation, four stages were defined (Figure 1):

- Stage I – Developmental stagnation: affected girls experience a normal growth until 6 to 18 months of age when they start manifesting a maturation stall. A typical feature of this stage is the slowed head development, generally associated to microcephaly. Other reported symptoms are postural weakness, hypotonia and loss of interest in the surrounding environment, with reduced eye contact. This pathology is frequently overlooked in this phase, leading to a late diagnosis.

- Stage II – Rapid regression: during the late infancy, affected children rapidly lose the previously acquired communication and motor coordination skills. Girls lose the purposeful use of hands that is substituted by stereotypical movements. In this phase, mental retardation and autistic-like features

become overt. Moreover, seizures and respiratory issues can often appear at this stage.

- Stage III – Pseudo-stationary stage: symptoms tend to stabilize in patients between 5 to 10 years of age. Improvement of communication skills and increased social awareness with intense eye gaze can be observed, even if intellectual abilities remain severely affected. During this period, girls can start suffering from autonomic issues, scoliosis and osteopenia.

- Stage IV – Late motor deterioration phase: after 10 years of age, patients often experience the loss of mobility and can become wheelchair-bound during teenage years. They often start to manifest parkinsonian features, osteoporosis and increasing severity of breathing and cardiac issues. As girls get older, symptoms become more static and patients can survive up to 60 years requiring total care due to their severely debilitated physical condition.

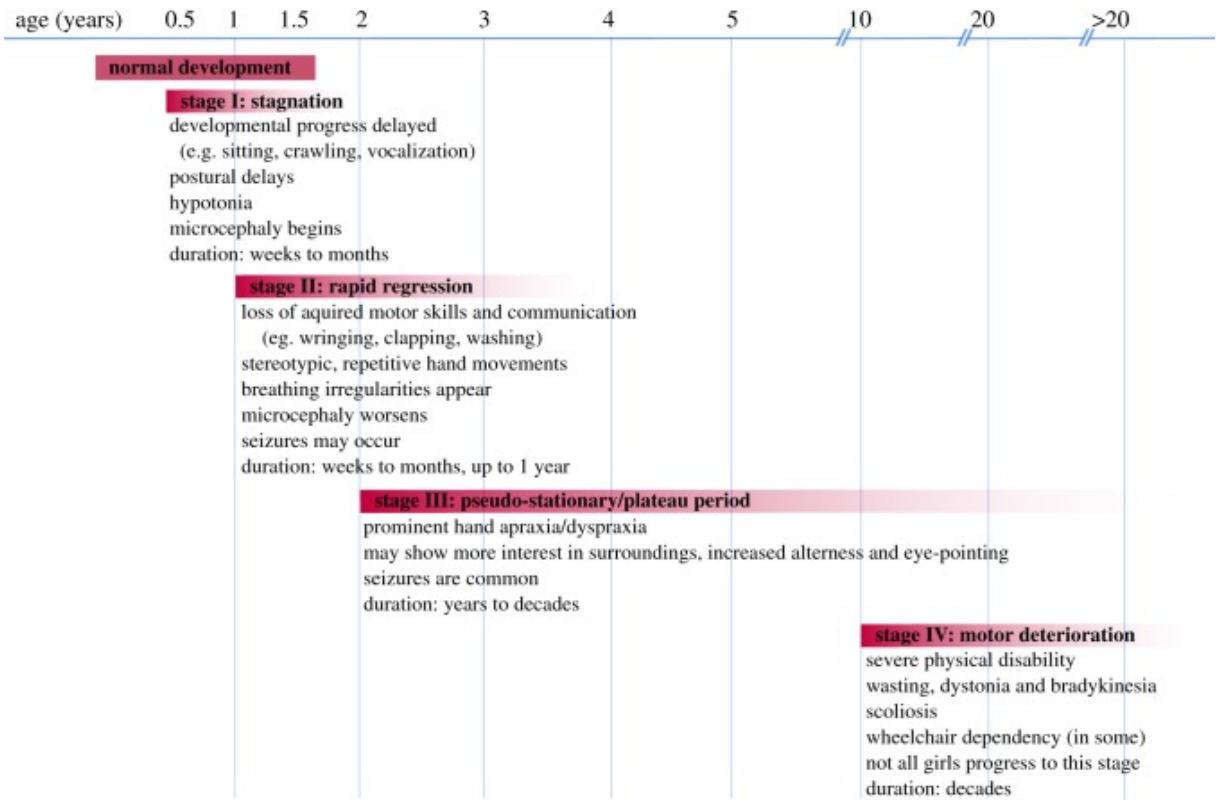

Figure 1. Timeline of stages in RTT progression. The figure illustrates the four stages of disease evolution, each characterized by the appearance of characteristic symptoms (Kyle et al., 2018) (5).

RTT symptoms occurrence and severity can vary between individuals, making the identification of the pathology in the earliest phases very challenging. Through the years, diagnostic criteria were re-edited many times until 2010, when Dr. Neul and colleagues established main and supportive characteristics to distinguish RTT from other neurodevelopmental disorders (6). Recognized diagnostic criteria serve also to discriminate classical forms of RTT from its variants, which are characterized by distinct clinical features. Of note, multiple cases have been described for three variant forms of RTT: the preserved speech variant, the congenital variant and the early seizure variant. The main feature for the diagnosis of both classical and variant RTT is the presence of a regression phase, followed by a stabilization. In addition, patients affected by classic RTT forms must manifest also other four key features, including the loss of acquired spoken language, loss of fine purposeful hand skills, gait abnormalities and hand stereotypic movements. Diagnosis for variant RTT forms requires at least 2 out of the 4 main criteria and other supportive symptoms, such as breathing problems, cardiovascular dysfunctions, growth retardation and scoliosis (Figure 2).

Requirement for classic or typical RTT	A period of regression followed by stabilization and recovery: 1. All main and all exclusion criteria 2. Supportive criteria not required although may be present
Requirement for variant or atypical RTT	1. A period of regression followed by stabilization and recovery 2. At least 2 of 4 main criteria and 5 of 11 supportive criteria
Main criteria	1. Partial or complete loss of acquired purposeful hand skills 2. Partial or complete loss of spoken language 3. Dyspraxic gait or inability to ambulate 4. Stereotypic hand movements: hand mouthing, hand wringing/clasping, hand clapping, or finger rubbing
Exclusion criteria	1. Brain injury: peri- or postnatal trauma, neurometabolic disease, or severe infection involving neurological function 2. Grossly abnormal psychomotor development in first 6 months after birth
Supportive criteria for variant RTT	1. Periodic breathing during wakefulness 2. Bruxism while awake 3. Altered sleep pattern 4. Abnormal muscle tone 5. Peripheral vasomotor disturbance 6. Scoliosis/kyphosis 7. Growth failure 8. Small cool/cold hands and/or feet 9. Inappropriate laughing or screaming spells 10. Delayed or diminished response to pain

Figure 2. RTT diagnostic criteria. The figure depicts the revised criteria required for the diagnosis of classic and variant forms of Rett syndrome. Diagnosis of classical forms of RTT requires the presence of all the main and the exclusion criteria, while supportive features may be present. For the diagnosis of atypical RTT manifestations at least 2 of 4 main criteria should be present, together with at least 5 of 11 supportive criteria (Percy et al., 2010) (7).

1.2 MECP2: the genetic driver of Rett syndrome

In 1999, Amir and colleagues identified the occurrence of *de novo* mutations in the X-linked *MECP2* gene as the cause of most of RTT cases (8). Currently, it is known that 95% of classic RTT cases and 75% of variant RTT cases are caused by *MECP2* mutations (9). *MECP2* gene encodes for Methyl-CpG-binding protein 2 (MeCP2), the founder member of the Methyl Binding Protein (MBP) family, a group of evolutionary conserved nuclear factors with the ability to bind DNA with at least one symmetrically methylated CpG-dinucleotide and generally involved in the epigenetic regulation of gene expression. The gene extends for ~ 76kb in the long arm of the X-chromosome (Xq28) and includes four different exons and three introns. Due to alternative splicing process, the gene is transcribed and spliced into two different isoforms, *MECP2-e1* and *MECP2-e2*, generating two proteins which only differ for the N-terminal part (10). Interestingly, the selective removal of e1 isoform in mice is sufficient to produce RTT-like phenotypes (11), while the lack of only Mecp2-e2 isoform does not result in the appearance of neurological defects (12). Of note, MeCP2-e1 is ten times more expressed than e2 both in mouse and human brain (4). Apart from the different N-terminal domain (NTD), both isoforms contain other four identical functional domains (13) (Figure 3):

- the methyl-CpG-binding domain (MBD, 91-174 aa);
- the intervening domain (ID, 175-218 aa);
- the transcriptional repressor domain (TRD, 219-322 aa), containing the nuclear localization signal (NLS);
- the C-terminal domain (CTD α and β, 323-498 aa)

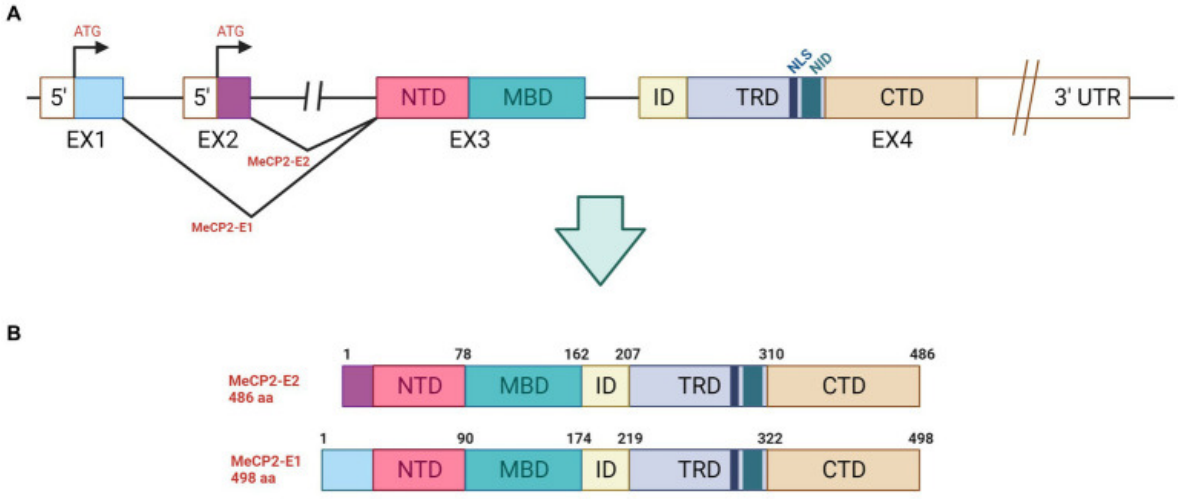

Figure 3 – MECP2 gene and MeCP2 protein. *MECP2* gene originates two protein isoforms through alternative splicing process. Both the isoforms, starting from the N-terminus (NTD), are composed by the Methyl-binding domain (MBD), the intervening domain (ID), the transcriptional repressor domain (TRD) and the C-terminal domain (CTD). Nuclear localization signals (NLS) are located in the ID and TRD domains (Palmieri et al., 2023) (14).

The different domains have been assigned to elucidate MeCP2 multiple functions, through direct DNA binding (MBD), interaction with protein partners or by recruiting other factors (mainly via TRD and CTD). Of note, MBD is the only domain showing a definite secondary structure, while the other domains (around 60% of the protein) are unstructured, thus conferring to MeCP2 the ability to interact with different partners and contributing to its multifunctionality (15) (16).

MeCP2 is a master regulator of gene expression

Given its interaction with methylated DNA and its capacity to suppress transcription, much of the research on MeCP2 structure has concentrated on its two primary functional regions: the MBD and the TRD. Through the MBD, MeCP2 binds methylated DNA displaying a preference for methylated cytosines found within mCpG or mCpA dinucleotides (17). Concurrently, the TRD mediates chromatin compaction at the level of MeCP2 binding sequences by engaging different transcriptional co-repressor complexes associated with histone deacetylase (HDAC) (18), including the Nuclear receptor Co-Repressor and the Silencing Mediator of Retinoic acid and Thyroid hormone receptor (the NCoR-SMRT complex). This interactions stimulates chromatin remodeling by eliminating acetyl groups from histone lysine residues (19). Furthermore, MeCP2 demonstrates the ability to suppress transcription in an HDAC-independent manner by recruiting the DNA methyltransferase DNMT1 and SUV39H1, an H3K9 histone methyltransferase, enhancing chromatin compaction (20). Within mature neurons, MeCP2 is also able to produce gene silencing through direct modulation of chromatin structure, since it can mimic the functioning of histone H1 by direct binding of the MBD to mCpGs, ultimately leading to chromatin condensation (21), (22). Beside this function as transcriptional repressor, it was subsequently discovered that MeCP2 can also act as a transcriptional activator for a subset of neuronal genes, by recruiting HDAC3 to deacetylate the transcription factor Forkhead box protein O3 (FOXO3) (23). In addition, it is reported that MeCP2 associates with

the cAMP-responsive element-binding protein1 (CREB1) selectively on active promoters and not on repressed sequences (24).
Notably, MeCP2 can regulate gene expression also indirectly, acting on alternative splicing process through the interaction with Y-box transcription factor 1 (YB1), a conserved RNA-binding protein (25) and with the spliceosome-associated protein PRPF3, the pre-mRNA processing factor 3 (26). The depletion of *Mecp2* in cortical neurons causes extensive alterations of mRNA splicing process, leading to intron retention and exon skipping (27). In addition, MeCP2 indirectly affects gene expression by regulating microRNA (miRNA) levels and subsequent gene silencing. In particular, it interacts directly with primary miRNAs at the mCpG-containing gene promoter regions through the MBD. Moreover, it can contact via its CTD the components of the microprocessor protein DiGeorge syndrome critical region 8 (DGCR8). As a result, the absence of MeCP2 leads to an increased primary miRNA transcription, which causes the increase of mature miRNA levels and gene silencing (27).

MeCP2 is involved in protein synthesis process

MeCP2 is also involved in the regulation of protein synthesis through the modulation of AKT/mTOR pathway, that is known to be fundamental for the formation of synaptic structures. An important downstream event of mTOR pathway is the phosphorylation of ribosomal subunit S6 (rpS6), that enhances ribosomal activity and increases the translation rate. The phosphorylation of S6 has been found consistently decreased in *Mecp2*-null mice brain tissues, resulting in impaired translation and reduced number and complexity of polysomes associated with mRNAs (28).

MeCP2 functions outside the nucleus

Our laboratory proved that MeCP2 can localize at level of the centrosomes of both dividing and post-mitotic cells. MeCP2 loss impairs the formation of mitotic spindle and affects microtubules nucleation process (29). The centrosome also gives origin to the primary cilium, a protruding organelle that works as a “sensory antenna” of differentiated cells. Thus, our laboratory further explored the centrosomal role of MeCP2 by examining the link between the protein and primary cilia, demonstrating that

the loss of MeCP2 affects ciliogenesis both in primary cultured mouse neurons and in the RTT mice brain (30).

Over the past five decades, a detailed examination of MeCP2's structure and functions has enabled the characterization of its numerous roles described above and summarized in Figure 4. However, many mechanisms governed by this complex protein remain still undiscovered.

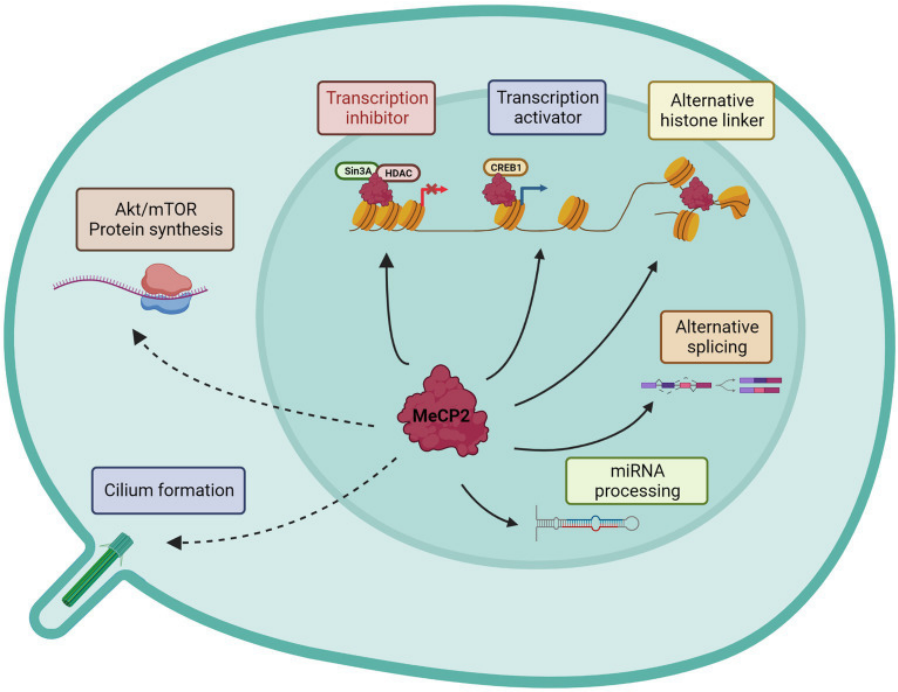

Figure 4 –MeCP2 is a multifunctional protein. MeCP2 can be considered a master regulator of gene expression, given its ability to act on transcriptional and post-transcriptional processes both directly and indirectly. Moreover, it plays other roles outside the nucleus, controlling centrosome functions, as mitotic spindle formation and ciliogenesis (Palmieri et al., 2023) (14).

1.3 Genotype – phenotype correlation

The majority of *MECP2* mutations originate spontaneously in the paternal germline, resulting in a disease occurrence that is predominantly sporadic (31). These mutations generally derive from C to T transitions probably related to the deamination of methylated cytosines (32). As previously mentioned, *MECP2* is located on the X chromosome, thus explaining the prevalence of female patients, showing a high phenotypic variability. In fact, X chromosome inactivation (XCI) process makes

heterozygous RTT patients mosaic for cells expressing either the wild type (WT) or mutant *MECP2* allele. The possible occurrence of skewed XCI can favor the expression of one allele or the other, thus affecting clinical severity (4). Beside XCI, symptoms variability is also influenced by the type of *MECP2* mutation. Up to now, over 900 unique variants have been identified within the gene, with the 55.8% being pathogenic mainly represented by frameshift mutations, insertion/deletions and missense mutations (33). Loss of function mutations in *MECP2* account for the vast majority of RTT cases, with a recurrence of 8 specific missense (R106W, R133C, T158M, R306C) and nonsense (R168X, R255X, R270X, R294X) mutations, distributed along the different domains of the gene (34). As a matter of fact, some genotype–phenotype correlation studies suggest that the *MECP2* mutation status can be used as a predictor of disease severity. Indeed, patients carrying the T158M or R106W missense mutations often exhibit more severe RTT phenotypes, while milder clinical manifestations are often associated with the presence of R133C or R306C mutations (35). Additionally, nonsense mutations located before or including R270X usually lead to more severe symptomatology (36) (Figure 5).

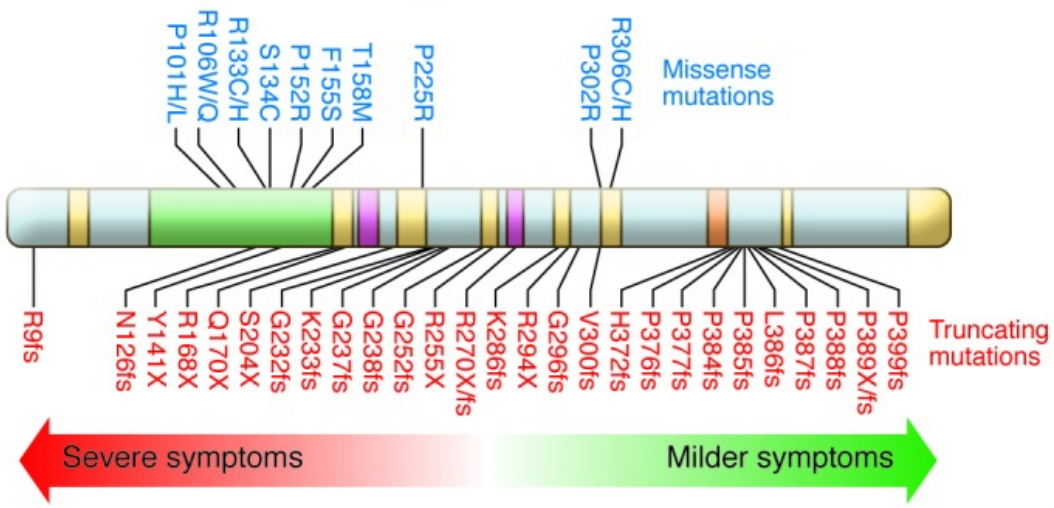

Figure 5 – Severity of RTT symptomatology depends on the position of MECP2 mutations. This figure depicts most frequent missense and truncating *MECP2* mutations. According to the gene region, mutations can be associated with a different severity of disease manifestations (Lombardi et al., 2015) (36).

Although RTT mainly affects females, some cases in males are documented: *MECP2* mutated hemizygous males generally present a severe phenotype, with frequent

infantile encephalopathy leading to death within the first years of life (37). Furthermore, *MECP2* hypermorphic mutations have been observed in male individuals affected by a severe intellectual disability known as MECP2 duplication syndrome (MDS) (38) leading to the premature death of patients before the age of 25 years. Interestingly, unlike Rett syndrome, males affected by MDS generally inherit the duplication from their mother, who carries the additional copy of the gene on a preferentially silenced X chromosome (39). Besides *MECP2*, mutations in other genes, such as X-linked cyclin-dependent kinase-like 5 (CDKL5; OMIM #300203) (40) or Forkhead box G1 (FOXG1; OMIM #164874) (41), have been associated with atypical and rarely classic forms of Rett. Although mutations in these genes are generally associated with other distinct pathologies, some mutations in *CDKL5* can be linked to the early-seizure onset variant of RTT, while mutations in *FOXG1* might result in the congenital variant (42).

1.4 Therapeutic strategies

To date, RTT remains without an effective cure and ongoing treatments are meant to alleviate symptoms. However, Bird and his team demonstrated that reintroducing *Mecp2* in symptomatic *Mecp2* KO animals led to the complete reversal of RTT phenotypes (43), suggesting that neurological deficits associated with RTT could not be permanent. Two different approaches have shown promise in alleviating disease symptoms:

1. *Directly acting on RTT genetic root:* given that RTT is a monogenic disorder caused by loss of function mutations in *MECP2*, gene delivery of a WT copy of the gene to mutant brain cells has been widely attempted (14). One of the major challenges related to this approach is the dosage-sensitivity nature of MeCP2, since its overexpression results in severe neurological defects (38). A significant breakthrough came from the study of Neurogene, based on the delivery of AAV9:*MECP2* into the cerebrospinal fluid, exploiting the Expression Attenuation via Construct Tuning (EXACT) technology. This technology allows the tuning of *MECP2* levels within a safe level, avoiding the toxicity related to its overexpression (44). Promising results were obtained both in mice and non-human primates and, in 2023, Neurogene claimed the approval of a clinical trial in female children with RTT (64). Similarly, a gene therapy strategy exploiting miRNAs to regulate the

overexpression of delivered *MECP2* showed promising results in preclinical studies and a clinical trial has been initiated in RTT females of 18 years or older (45). Other strategies that are currently under investigation are based on *MECP2* gene and RNA editing with CRISPR-Cas9 (46,47), reactivation of the inactive X chromosome (48) and readthrough of MECP2 nonsense codon mutations (49,50).

2. *Targeting MeCP2 downstream pathways:* researchers also focused on the restoration of biological pathways deeply affected by MeCP2 dysfunction, as neurotransmission, metabolism and growth factors expression. Even though many approaches were successful in preclinical studies, the only approved drug for RTT up to now is Trofinetide, a synthetic analogous of N-terminal active tripeptide (Glutamate-Proline-Glycine, GPE) of Insulin Growth Factor 1 (IGF1), a fundamental neurotrophin for neuronal maturation and synapse formation (51–54). Its safety and tolerability were assessed in a phase II trial (NCT02715115), that also reported the efficacy of the drug to ameliorate stereotypic movements, mood dysfunctions and ambulation (55). These encouraging results led to a successful randomized double-blind placebo-controlled phase III LAVENDER trial (NCT04181723) proving Trofinetide efficacy and safety in RTT girls (from 5 to 20 years of age), with reported ameliorations in communication, motor skills and use of hands (56).

1.5 Neurobiology of RTT

Neurological defects constitute primary symptoms of RTT and extensive effort has been employed to characterize anatomical, molecular and functional alterations within the central nervous system (CNS).

Morphological defects

It has been estimated that almost 98% of RTT patients exhibit slower head development with resultant microcephaly (57). This reduction in brain dimension generally occurs two months after birth, in the absence of any neurodegeneration sign (58,59). Investigations on post-mortem brain tissues and MRI analyses unveiled the presence of a widespread cortical thinning and reduction in the volume of both grey and white matter, mainly concerning prefrontal, posterior frontal and anterior temporal regions (4) (59). Further histological examinations of RTT post-mortem tissues

revealed decreased neuronal cell size and increased cell density in cortical and subcortical brain regions, alongside reduced dendritic complexity in hippocampal pyramidal neurons as well as in frontal and motor cortices (60). Furthermore, a decreased number of synapses and spine density have been reported in human samples (61,62). Of relevence for the preclinical research, all of these morphological and functional defects are present across various lines of *Mecp2* mutant mice. Actually, mouse models of RTT start displaying a widespread reduction in brain size and cortical thickness at 4 weeks of age (63,64) and their neurons exhibit smaller soma size, increased packing density, reduced dendritic arborization and number of spines in multiple brain regions, including the hippocampal CA1 region as well as the motor and somatosensory cortex (65,66). According with the early expression of MeCP2 (67,68), morphological alterations are even present in immature (DIV3) primary neurons derived from E15.5 *Mecp2* KO mice embryos (67), highlighting the crucial role of this protein since the earliest stages of development. These evidences are in line with the reported expression of MeCP2 in human brainstem and cerebral cortex after three months of gestation (69) and with the neurological impairments shown by RTT patients in the first years of life (70).

Neurochemical defects

Several neurochemical alterations have been described both in RTT patients and mouse models. Indeed, magnetic resonance spectroscopy analysis indicated that levels of excitatory neurotransmitter glutamate are elevated in brain and in the cerebrospinal fluid (CSF) of RTT patients (71,72). Studies on post-mortem brain tissues indicated that densities of N-methyl-D-aspartate (NMDA) and α-amino-3-hydroxy-5-methyl-4-isoxazolepropionic acid (AMPA) glutamate receptors are above control levels in the frontal cerebral cortex and basal ganglia of young patients (from 2 to 8 years) (73). In line with these clinical evidences, *Mecp2* KO mice show significantly higher levels of glutamate in the frontal cortex with respect to control animals (74). Additionally, a singificant decrease in the level of biogenic amines, dopamine and serotonine, was reported in the CSF of 2 to 15 years of age RTT patients (75). Also Wenk and colleagues found decreased endogenous levels of dopamine and its metabolites in the neocortex and basal ganglia of RTT brains (76). Interestingly, *Mecp2* deletion from dopaminergic neurons caused severe locomotor abnormalities in

conditional KO mice, while removing the protein from serotoninergic neurons caused anxiety, aggressive behavior and altered sociability (77). Another reported alteration in RTT patients is the increased level of choline in brain unveiled by magnetic resonance spectroscopy analysis (78) and the importance of Mecp2 role in the cholinergic system is further confirmed by the removal of the gene selectively from cholinergic neurons that causes an impairment of social behavior and seizures occurrence (79). The described widespread alterations of neurotransmitters level in RTT brains deeply impact on neuronal circuits functioning, as shown by reported abnormal somatosensory evoked potentials and electro-encephalograms (EEG) (4,80). In line with this, *Mecp2* mutant mice show an altered excitatory/inhibitory (E/I) balance in different brain areas. In particular, a reduction in cortical excitability was detected in 2 weeks old *Mecp2* KO mice and the described phenotype worsened when first RTT symptoms appeared at 5 weeks (81). These findings were reinforced by the reported 40% reduction in the number of functional excitatory glutamatergic synapses in the cortex of *Mecp2* KO animals (82). On the contrary, a shift towards hyperexcitation was detected in acute slices of CA3 hippocampal region from symptomatic *Mecp2* KO mice, with a reported decrease γ-aminobutyric acid (GABA) receptors and increased number of ionotropic glutamate receptor GluA1 subunits (83). To further depict the role of Mecp2 in inhibitory and excitatory circuits, *Mecp2* gene was conditionally deleted from either GABAergic or glutamatergic neurons in mice. The deletion of *Mecp2* from GABAergic neurons was sufficient to induce the development of motor and cognitive impairments (84), while the selective removal of *Mecp2* from excitatory glutamatergic neurons caused the onset of anxious behavior and tremor (82).

Transcriptomic and proteomic defects

Despite the advances in understanding neurological alterations due to MeCP2 dysfunctions, only few target genes have been directly linked to RTT pathogenesis. This is likely due to the fact that MeCP2 finely regulates the expression of thousand genes and it is also involved in chromatin compaction process (13,21). Consequently, RTT models exhibit broad transcriptional alterations, although the magnitude of these changes is often subtle. For this reason, many studies focused on the analysis of gene sets and pathways to gain insight on the most affected cellular processes in RTT (85,86). Synaptic plasticity and function, together with neuronal inhibitory and

excitatory activity are the functional networks that are consistently altered in RTT human post mortem brain tissues, in RTT mouse models and in patients-derived induced pluripotent stem cells (iPSCs) (87–90). Moreover, many genes involved in neuronal maturation and cortical development were found deregulated in embryonic cortical neurons from *Mecp2* KO mice (67). One of the genes involved in neuronal maturation and synaptic functioning that is stably downregulated in RTT models is the brain-derived neurotrophic factor (BDNF) (91). The involvement of BDNF in RTT pathogenesis has been supported by the generation of a conditional KO mice for *Bdnf*, which exhibited many RTT-like symptoms. Moreover, Bdnf overexpression in *Mecp2* KO mice improved lifespan and locomotor activity (92,93). Considering other differentially expressed gene sets in RTT samples, inflammation related genes are often found upregulated, thus underscoring the subclinical inflammatory status characterizing the pathology (94–97). In particular, *Irak1*, a kinase involved in the activation of the nuclear factor kappa-light-chain-enhancer of activated B cells (NF-κB) pathway and mediating the expression of pro-inflammatory cytokines, was found consistently upregulated in several transcriptional profiles conducted on *Mecp2* mutant samples (95). Likewise, genes enriched in tumor necrosis factor (TNF) signaling pathway appear upregulated in *Mecp2* KO embryonic cortical neurons, further underlining the presence of an altered immune response (98). Other pathways that are commonly deregulated both in RTT patients and *Mecp2* KO mice brain tissues are related to lipid metabolism, cholesterol production and mitochondrial functionality (99,100). In line with this evidence, RTT is characterized by profound metabolic dysfunctions and patients display dyslipidemia, altered content of cholesterol in serum and increased oxidative stress (5).

Even if RNA sequencing analysis provided much information on RTT pathogenesis, it is important to consider that proteostasis is totally disrupted in this pathology, due to the fundamental role of MeCP2 in the regulation of protein synthesis (28). Thus, analysis of the proteome in RTT patients samples and *Mecp2* mouse models could provide a more complete understanding of disease biology. Of relevance, Pacheco and colleagues integrated transcriptomic and proteomic analyses on the cortices of P60 KO mice, revealing a significant dysregulation of 35 gene-protein “hits” in RTT mice. In line with described neurobiological defects, these factors are involved in synaptic functions, neurotransmission, neuronal morphology and development. This work also underlined the inflammatory dysregulation characterizing the pathology, reporting an

alteration of cytokine production and CNS inflammation (101). Noteworthy, a metabolic impairment emerged from a proteomic analysis run in patients-derived fibroblasts, where Cicaloni and colleagues found altered expression of proteins related to respiratory chain activity, oxidative stress and mitochondrial dynamics (102).

1.6 Astrocytes role in RTT pathogenesis

Many of the described alterations are not exclusively caused by MeCP2 mutations in neuronal cells, but they derive from functional defects arising in other cell types, that are equally important for correct brain functioning. Notably, most studies on RTT have focused on neurons as MeCP2 was initially believed to be expressed exclusively in this cells, reaching its highest levels at the end of neuronal maturation (69). However, MeCP2 expression was subsequently detected in neuroglia, a population of cells encompassing oligodendrocytes, microglia and astrocytes (103,104). Among them, astrocytes, named for the star-like appearance, were at first mainly considered as mere supporting cells for neurons. Conversely, they are now known to play many other fundamental roles in CNS functioning (105). Indeed, astrocyte – neuron communication is a crucial mechanism for correct synaptogenesis, synaptic functioning, fine tuning of neuronal activity and neuronal energy metabolism (106), mechanisms that are deeply impaired in RTT. It is now clear that MeCP2 mutations directly impact also astrocyte morphology and functioning, which indirectly affect neurons through a non-cell-autonomous mechanisms (107). Adding a layer of complexity to the studies on RTT, it is important to mention that the brains of RTT patients are a mosaic for astrocytes and neurons (and all the other cell types) expressing either the WT protein or the mutant one (108). Further studies are needed to determine and discriminate the contribution of the individual cell genotype (cell-autonomous effects) and of the surrounding environment (non-cell-autonomous effects) to the development of RTT phenotypes.

1.6.1 Astrocyte – neuron communication in physiological conditions

To better understand astrocyte – neuron communication impairment in RTT, it could be useful to have a quick overview on this complex mechanism in physiological conditions. Importantly, this communication mechanism works in a bidirectional way. Indeed, astrocytes locally respond to adjacent neuronal activity, developing a

substantial molecular and functional diversity (109). However, the majority of evidence describes the effects exerted by astrocytes on neurons, elicited both through the direct contact between these cells and the release of signaling molecules, named gliotransmitters. In details, through their peripheral processes, which enwrap pre- and post-synaptic terminals (110) composing the tripartite synapse (Figure 6), astrocytes finely control the concentration of ions and molecules, regulating synapse activity and avoiding excitotoxicity. Moreover, when activated by internal or external triggers, astrocytes generate transient elevations of Ca^{2+} levels (111), resulting in the release of a plethora of diverse signals to neighboring neurons, regulating many different aspects of their functioning (112,113).

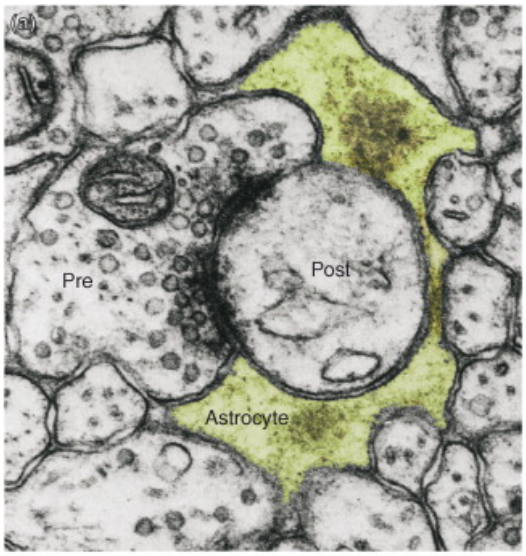

Figure 6 – Tripartite synapse. Electron micrograph of a pre-synaptic (Pre) and post-synaptic (Post) terminal enwrapped by the astrocytic process (green) forming the structure of tripartite synapse (Halassa et al., 2007) (114).

Modulation of synaptic activity

At the synaptic cleft, astrocytes can synthesize and release glutamate *de novo* from glucose (115,116), but they are also responsible for the reuptake of this neurotransmitter through the amino acid transporters GLAST1 (glutamate-aspartate transporter 1) and GLT-1 (glutamate transporter 1), and the human homologous EAAT1 and EAAT2, respectively. Then, internalized glutamate is converted by glutamine synthetase to glutamine, that is released and exploited by either excitatory neurons to produce glutamate or by inhibitory neurons to synthetize GABA (117,118). Importantly,

astrocytes are also in charge to remove GABA from the synaptic cleft through the GABA transporters GAT-1 and GAT-3 (119) but they can also secrete GABA and glycine, thus modulating inhibitory transmission (120,121). Astrocytes also release neuromodulators as the amino acid D-serine, that is able to bind to N-methyl-D-aspartate (NMDA) receptor mediating excitatory transmission and long term potentiation (LTP) process (122). Also inflammatory molecules produced by astrocytes are involved in the regulation of synaptic activity. Indeed, Tumor Necrosis Factor α (TNFα) increases AMPA receptors number on the excitatory synapses and decreases $GABA_A$ receptors at inhibitory synapses (123,124). Moreover, astrocytes control the concentration of ions at synaptic cleft and this is particularly important in order to prevent hyperexcitability during intense neuronal activity when K+ levels rise extracellularly (125). Potassium channels (Kir4.1) contribute to buffer extracellular potassium and avoid neuronal circuits damage (126).

Energetic support

Furthermore, astrocytes provide essential energy substrates to neurons through the astrocyte-neuron lactate shuttle. In details, astrocytes uptake glucose from the blood flow to convert it to lactate through glycolysis. Lactate is released in the extracellular space and internalized by neighboring neurons to produce the necessary ATP for synaptic activity (127–129). Another way by which astrocytes support neuronal activity is through the formation of the neurovascular unit at the blood brain barrier (BBB) level, where they respond to local needs, secreting different mediators such as prostaglandins, nitric oxide and arachidonic acid (130). These molecules contribute to modify the diameter of blood vessels, regulating the local blood flow to ensure that active brain regions receive sufficient oxygen and nutrients (131).

Induction of synaptogenesis

Beyond synaptic function, synaptogenesis is another process finely regulated by astrocytes. Indeed, several molecules produced by astrocytes are known to promote the formation of excitatory synapses. Among these, the first identified was cholesterol which increases the formation of synaptic vesicles at the pre-synaptic terminal and stabilizes the level of NMDARs receptors at post-synaptic side (132,133). Other well

studied synaptogenic molecules secreted from astrocytes during development include the thrombospondins 1 e and 2 (TSP1, TSP2), which are able to bind the synaptogenic pre-synaptic calcium channel subunit α2δ1 (Cacna2d1) (134), and the extracellular matrix component glypican 4 (Gpc4), which is sufficient to induce the recruitment of AMPA receptors at synapse level, stimulating excitatory transmission. Astrocytes are also able to induce the formation of inhibitory synapses (135,136), even if the involved factors remained elusive for over a decade and are mostly still unknown. Very recently, Irala and colleagues highlighted the involvement of neurocan (NCAN) in the formation of inhibitory synapses of somatostatin positive interneurons. NCAN is mainly produced from astrocytes during synaptogenesis and it is cleaved in two halves: the N-terminal part participates to the formation of perineuronal nets, while its C-terminal portion is released in the extracellular matrix and binds several proteins expressed from inhibitory neurons, finally promoting the formation of new inhibitory synapses (137).

Neuronal activity shapes astrocytes functioning

As mentioned before, also astrocyte functioning is deeply influenced by neurons, but the mechanisms are yet poorly understood. What is known is that, when cultured in absence of neurons, astrocytes maintain a polygonal shape and only express the glutamate transporter GLAST. Neurons are able to induce the classic stellate morphology in astrocytes and trigger the expression of GLT-1 (138). Moreover, neurons can induce the expression of connexins composing the gap junctions in astrocytes, thus promoting their functional maturation (139). Hasel and colleagues uncovered the transcriptional changes associated to the astrocytic maturation induced by the presence of neurons. In detail, they found that the neuron-derived Notch signaling pathway mediates the process of neurotransmitters release and metabolism (109). Moreover, the synaptic activity triggers the upregulation of genes mediating glucose metabolism and lactate shuttle process (109,140). Importantly, neurons also significantly impact astrocyte Ca^{2+} dynamics. Indeed, astrocytes sense synaptic activity through the activation of metabotropic or ionotropic receptors that in turn causes variations of astrocytic intracellular Ca^{2+}, triggering the release of different gliotransmitters (141–143). Different levels of synaptic activity trigger Ca^{2+} elevations in astrocyte with various spatio-temporal characteristics, demonstrating the direct effect of neuronal signaling on astrocytes (144).

All in all, collected evidence confirms the close functional and metabolic coupling between astrocytes and neurons. Impairment of this complex bidirectional communication results in the occurrence of diverse neurodevelopmental and neurological disorders (145,146).

1.6.2 Astrocyte – neuron communication in RTT

The first evidence of astrocytes' involvement in RTT pathogenesis emerged in 2009, when Ballas and colleagues discovered that *Mecp2* KO astrocytes failed to support the correct development of neuronal morphology. In particular, hippocampal neurons cultured in contact with *Mecp2* KO cortical astrocytes showed a significant reduction in their dendritic length if compared to neurons exposed to WT astrocytes. This evidence indicates that the presence of MeCP2 in astrocytes is fundamental to ensure correct neuronal maturation. In addition, WT neurons exposed to the astrocyte conditioned medium (ACM) of *Mecp2* KO astrocytes for 6 days exhibited stunted dendritic morphology, thus unveiling the pivotal role of the factors secreted by astrocytes in the development of RTT phenotypes (103). Following this evidence, to better dissect the role of astrocytes in this pathology, *Mecp2* expression was selectively reactivated in astrocytes of a conditional KO mouse model and this was sufficient to improve motor skills, ameliorate breathing and significantly prolong mice lifespan (147). Moreover, hippocampal astrocytes appeared atrophic after *Mecp2* full conditional removal in juvenile mice (5 weeks of age), demonstrating the importance of Mecp2 expression for physiological astrocyte development (148). In line with these data, genes related to astrocyte maturation and morphology have been found deregulated in P60 *Mecp2* KO mice (101) and cytoskeletal alterations have been reported in this model already at P20, when RTT phenotypes are not overt. The same defects are present in symptomatic heterozygous *Mecp2*$^{+/-}$ females (HET), despite their mosaicism (149). Morphological anomalies have been documented also in post mortem brains of two female RTT patients carrying R225X mutation, where astrocytes show a dramatic reduction of their structural complexity (150). Altered morphology caused by the absence of MeCP2 in astrocytes deeply influences the correct functioning of neighboring neurons, as demonstrated by culturing hiPSCs derived astrocytes carrying mutations in *Mecp2* gene (V247X, R294X and R306C) with mouse hippocampal neurons. Neurons not only showed altered dendritic branching and

smaller soma size but also reduced miniature excitatory postsynaptic currents (mEPSCs). Interestingly, the same results are obtained by exposing neurons to the ACM collected from generated RTT astrocytes, thus reinforcing the evident contribution of secreted molecules in determining neuronal defects (151). Moving to a more complex model, dual patch clamp of astrocytes and neurons in *Mecp2* KO brain slices revealed a reduced calcium signaling in cortical astrocytes and a strong impairment in the astrocyte-mediated synaptic transmission in neurons. To determine whether the defective signaling was due to the neuron itself or to astrocytes (or both cell types), researchers exploited brain slices collected from HET animals, where they found that neuronal transmission proceeds correctly only when the astrocyte expresses Mecp2 (152). Therefore, synaptic activity is deeply influenced by the presence of Mecp2 in astrocytes, underlining the importance of non-cell autonomous mechanisms for correct brain functioning. Given the rising evidence on the involvement of astrocyte secreted factors in RTT, research groups started to focus on the characterization of *Mecp2* mutant astrocyte conditioned medium (ACM), hypothesizing an increased release of toxic factors or the reduced secretion of beneficial molecules. Quantitative mass spectrometry analysis run on ACM from mouse primary cultures of WT and *Mecp2* KO astrocytes revealed 29 differentially expressed proteins: up-regulated targets are mostly involved in inflammatory response, complement activation, positive regulation of neuron death and metabolic process, while the down-regulated proteins are related to apoptosis, maintenance of protein location, cellular response to Interleukin-1 (153). Other interesting data on the composition of RTT ACM came from Caldwell and colleagues, who performed proteomic analysis on the secretome collected from astrocytes immunopanned from the cortex of RTT, Fragile X and Down syndrome mouse models. The study revealed a common aberrant expression of the Insulin-like growth factor binding protein 2 (Igfbp2) that contributes to the stunted dendritic branching of neurons by inhibiting the activity of IGF1 and an alteration in astrocytes of Bone Morphogenetic Protein 6 (BMP6), that impairs astrocyte maturation (54,154). Moreover, in *Mecp2* KO ACM they found increased release of Semaphorin3f (Sema3f), that is known to inhibit dendritic outgrowth (155). Further analysis of *RTT* astrocytes secretome revealed also metabolic anomalies. Untargeted ^{1}H NMR reported a significant increase in lactate and decreased amount of pyruvate in the ACM collected from hiPSCs differentiated in astrocytes carrying *MECP2* R270X mutation. This evidence is mirrored by the decreased amount of

tricarboxylic acid (TCA) cycle intermediates and the lower amount of ATP produced in RTT astrocytes with respect to WT cells, finally explained by a mitochondrial dysfunction (156). Despite the increasing number of data collected to date, one of the major limitation of the described studies is that the proteomic and metabolomic analyses have been performed on the secretome collected from astrocytes cultured alone, without considering the influence elicited from neurons on astrocyte morphology, gene expression and functioning. This issue is particularly relevant in RTT brains, characterized by mosaic interactions between astrocytes and neurons expressing either the WT or the *MECP2* mutant allele. In this context, *MECP2* mutations not only cause intrinsic defects in astrocytes and neurons, but also affect neighboring cells through non-cell-autonomous communication mechanisms, thus contributing to the development of RTT symptoms.

2. Aim of the thesis

Many studies in Rett syndrome (RTT) highlighted the pivotal role of astrocytes in the pathogenesis of the disease. It has been reported that *MECP2* mutations in astrocytes cause cell-autonomous defects, altering cell morphology, gene expression and functioning. These alterations make *MECP2* mutant astrocytes defective in supporting neuronal development, thus participating to the emergence of the typical synaptic defects and altered neurotransmission characterizing RTT brains. Since many functions of astrocytes are exploited through the release of gliotransmitters eliciting non-cell-autonomous effects on neighboring neurons, proteomic and metabolomic analyses of astrocyte conditioned medium (ACM) collected from *MECP2* mutant astrocytes unveiled a plethora of differentially expressed molecules, which could be responsible for the detrimental effect on neuronal morphology and activity. In our laboratory, we observed that treating WT neurons with *Mecp2* knock-out (KO) ACM reduces the number of pre- and post-synaptic markers, as well as their colocalization, which is considered an index of active synapses. This phenotype could result both from the lack of beneficial cues and the presence of synaptotoxic factors in the conditioned medium, thus studying ACM composition might inform on the nature of the involved secreted molecules. However, in physiological conditions, astrocytes are not alone but strictly connected with neurons, which influence transcriptional, morphological and functional features of astrocytes. For this reason, the mere characterization of ACM could be limiting, without highlighting those factors deregulated only when a communication between astrocytes and neurons is preserved. To overcome this drawback, we also included in our study a co-culture between astrocytes and neurons, in which astrocytes are seeded on transwell inserts and maintained above neurons for 14 days. This system permits the exchange of secreted molecules between glial and neuronal cells, but prevents their direct contact, thus allowing to specifically study non-contact communication mechanisms. As observed after ACM treatment, we found that also in co-culture with *Mecp2* null (KO) astrocytes, WT neurons show a decrease in pre- and post-synaptic markers and their colocalization, confirming the inability of RTT astrocytes to sustain synaptogenesis. Thus, exploiting the two different *in vitro* systems, in my PhD project, I aimed at identifying the factors secreted by KO astrocytes that contribute to the alteration of synaptic phenotype, with the final aim of

finding promising molecular targets for the development of novel therapeutic strategies for RTT.

3. Materials and methods

3.1 Animals

3.1.1 Animal care and genetically modified mouse lines

Mice are housed in the animal facility of the L.I.T.A building of the University of Milan. Animals are housed in groups of two/three for each cage, in a temperature- and humidity-controlled environment (21 ± 2 °C) and a 12-hour light/dark cycle, with food and water *ad libitum*. All procedures conducted on mice are performed in accordance with the European Community Council Directive 2010/663/UE for care and use of experimental animals and Italian laws (D.L.26/2014). Protocols are approved by the Italian Council on Animal Care in accordance with the Italian law (Italian Government decree No. 187/2022).Two different mouse lines are used in this study: the *Mecp2* null mouse strain developed by Guy and colleagues (157) and the *Mecp2* knock-in (KI) Y120D mouse line generated in our laboratory and characterized by Gandaglia and colleagues (158). The Mecp2$^{tm1.1Bird}$ mouse strain is purchased from the Jackson Laboratories. It lacks Mecp2 protein due to deletion of exons 3 and 4. Hemizygous *Mecp2* knock-out (KO) male mice appear normal at birth until 4 weeks of age, when they show a rapid regression and start manifesting neurological symptoms, as motor defects, abnormal gait, hind limb clasping, tremors and breathing irregularities (63). These features progressively get worse, reducing lifespan, which rarely reaches more than three months of age (159). Heterozygous females, *Mecp2*$^{+/-}$ (HET), display milder phenotypes and a slower disease progression: indeed, symptoms become overt after 3-4 months of age and their lifespan reaches at least 10 months (36). Due to skewed XCI the severity of their phenotype can vary (159). Of relevance, KO mice are sterile, while HET females remain fertile and are mated for colony maintenance. The original *Mecp2*$^{tm1.1Bird}$ strain created in a C57BL/6 background is characterized by poor maternal care, low number of pups per litter and frequent events of litter cannibalism. To overcome this limitation, our laboratory transferred the *Mecp2*$^{tm1.1Bird}$ strain on an outbred CD1 genetic background, obtaining large litters, with very low frequency of cannibalism. The mice maintain RTT-like phenotypes displayed by the BL/6 strain at the behavioral and molecular levels (160).

The other model used for this study is a KI *Mecp2*^{Y120D} mouse, generated in our laboratory and mimicking the mutation found in a Japanese RTT girl. Phenotypically,

these mice develop a severe RTT-like behavior, reproducing the RTT-like features displayed by KO mice, even though they diverge at the molecular level (158).

3.1.2 Genotyping

Genotyping is performed by Polymerase Chain Reaction (PCR) protocol on genomic DNA purified from ear biopsies of P20 mice or paws/tails of embryos and P0-P3/P7 pups.

DNA extraction from biopsies of P20 animals

Ear biopsies are dissociated with Lysis Buffer (Tris 100mM pH=8, EDTA 10mM pH=8, SDS 0.5%, NaCl 100mM) and Proteinase K (0.5 mg/mL) maintained overnight at 55° C. The day after, samples are centrifuged (13,000 rpm, 10 minutes) to remove any debris. Then, 1:1 of 100% isopropanol is added to the supernatants to induce DNA precipitation at room temperature (RT) (13,000 rpm, 10 minutes). Supernatants are removed and DNA pellets are washed with 500µL of 70% ethanol (EtOH) and centrifuged at 13,000 rpm for 5 minutes. EtOH is eliminated, pellets are dried at RT and resuspended in 50µL of water for DNA quantification, performed with a spectrophotometer (Nanodrop 1000, ThermoFisher).

DNA extraction from biopsies from embryos and pups

Tissues are dissociated with “Phire animal tissue direct PCR kit” to rapidly extract DNA from samples dedicated for primary cultures. In detail, each sample (mouse paw or tail) is incubated with a 20 µL mix (19.5µL Dilution Buffer + 0.5µL DNA Release Additive provided by the “Phire animal tissue direct PCR kit”) for 3 minutes at RT. Then, the reaction is stopped at 98°C for 2 minutes and supernatant is diluted with 10µL of the Dilution Buffer and directly used for DNA quantification. For embryonic samples, PCR for both genotype (WT or mutant Mecp2) and sex (for the Y-linked Jarid gene) is conducted.

PCR and gel electrophoresis:

The reaction mix for one sample (Final volume = 20µL) for PCR amplification is the following (Table 1)

Mecp2 protocol			
Reagents	**Initial concentration**	**Final concentration**	**Final volume**
Xtra RTL GL Reaction Buffer	5X	1X	4µL
dNTPs	10mM	10µM	0.4µL
Reverse primer	10µM	0.25µM	0.5µL
Forward primer (WT allele)	10µM	0.25µM	0.5µL
Forward primer (null allele)	10µM	0.25µM	0.5µL
XtraTaq Pol RTL	5U/µL	0.125U/µL	0.5µL
H_2O	–	–	12.6µL
gDNA	100ng	5ng/µL	1µL

Mecp2 Y120D protocol			
Reagents	**Initial concentration**	**Final concentration**	**Final volume**
Xtra RTL GL Reaction Buffer	5X	1X	4µL
dNTPs	10mM	10µM	0.4µL
Forward primer	10µM	0.25µM	0.5µL
Reverse primer	10µM	0.25µM	0.5µL
Reverse primer (mutant allele)	10µM	0.25µM	0.5µL
XtraTaq Pol RTL	5U/µL	0.125U/µL	0.5µL
H_2O	–	–	12.6µL
gDNA	100ng	5ng/µL	1µL

Jarid protocol (for sex determination)			
Reagents	**Initial concentration**	**Final concentration**	**Final volume**
Xtra RTL GL Reaction Buffer	5X	1X	4µL
dNTPs	10mM	10µM	0.4µL
Forward primer	100µM	0.625µM	0.125µL
Forward primer	100µM	0.625µM	0.125µL
XtraTaq Pol RTL	5U/µL	0.125U/µL	0.5µL
H_2O	–	–	13.85µL
gDNA	100ng	5ng/µL	1µL

Table 1: ***PCR mix for genotyping Mecp2$^{tm1.1Bird}$ and Mecp2^{Y120D} mouse lines and for the determination of sex.***

Negative control (19µL reaction mix + 1µL of Dilution Buffer or H_2O) and positive controls (19µL reaction mix + 1µL DNA of a heterozygous, WT and mutant mice) are always included.

The primers used for the genotyping are the following:

- For *Mecp2*$^{tm1.1Bird}$ mouse line:
    - common reverse primer: 5' CCACCCTCCAGTTTGGTTTA-3';
    - forward primer for wild-type allele: 5'GACTGAAGTTACAGATGGTTGTG-3';
    - forward primer for null allele: 5'-ACCTAGCCTGCCTGTACTTT-3'.
- For *Mecp2* ^{Y120D} mouse line:
    - common forward 5′–CAGGGCCTCAGAGACAAGC–3′;
    - common reverse 5′–GCAGATCGGCCAGACTTCC–3′;
    - reverse for the KI allele 5′–GGGTTAATTGATATCCAATTGGGATCC–3′.
- For sex determination:
    - *Jarid1* forward 5′–CCAGGATCTGACGACTTTCTACC–3′;
    - *Jarid1* reverse 5′–TTCTCCGCAATGGGTCTGATT–3′.

The PCR cycles are reported in Table 2.:

Step	*Mecp2* KO	*Mecp2* Y120D	Jarid
Heat lid	110°C	110°C	110°C
Denaturation	94.0°C (5 min)	95.0°C (2 min)	95.0°C (2 min)
Start loop	35X	35X	35X
Denaturation	94.0°C (30sec)	95.0°C (30sec)	95.0°C (30sec)
Annealing	60.0°C (30 sec)	60.0°C (30 sec)	59.0°C (30 sec)
Extension	72.0°C (1 min)	72.0°C (45 sec)	72.0°C (30 sec)
Close loop	–	–	–
Final extension	72.0°C (5 min)	72.0°C (5 min)	72.0°C (5 min)
Hold	4°C (∞)	4°C (∞)	4°C (∞)

Table 1: PCR cycles for genotyping and sex determination.

PCR products are resolved by electrophoresis run in 2% agarose gel (110V, 40 minutes run in TAE 1X buffer).

- For *Mecp2*$^{tm1.1Bird}$ strain: WT mice present a band of 411 bp, while *Mecp2* KO mice present a band of 458 bp. Heterozygous mice exhibit both bands, one for each allele.
- For *Mecp2*^{Y120D} strain: A 300 bp fragment is common for WT and KI animals, while a 550 bp fragment is specific for the mutated one.
- For sex determination: the amplification of *Jarid1* produces a fragment of 113 bp only in males.

Materials

- 2-Propanol, SIGMA, cod. 33539
- Agarose LE, GENESPIN, cod. STS-AG500
- Deoxynucleotide Set, 100 mM, SIGMA, cod. DNTP100A
- Ethylenediaminetetraacetic acid (EDTA), SIGMA, cod. EDS
- Ethanol (EtOH), SIGMA, cod. 32221
- Nuclease-Free Water, SIGMA, cod. W4502
- Phire animal tissue direct PCR kit, Thermo Scientific, cod. F140WH
- Proteinase K, GENESPIN, cod. STS-OK500
- SYBR Safe DNA Gel Stain, Thermo Scientific, cod. S33102
- Trizma base, SIGMA, cod. 93352
- Xtra RTL GL Reaction Buffer, GENESPIN, cod. XSTS-T5XRTL GL
- Xtra Taq Pol, GENESPIN, cod. XSTS-T5XRTL GL

3.2 Primary cultures

3.2.1 Primary cultures of cortical neurons

The day of vaginal plug is considered E0.5 and primary cortical neurons are prepared from WT, *Mecp2* KO and HET mouse embryos at E15.5. Embryos are sacrificed by decapitation and brains are removed under a stereomicroscope and immersed in ice-cold Hank's Buffered Salt Solution (HBSS). Meninges are removed and cerebral cortex is dissected and maintained in cold HBSS until tissue dissociation. Tissues are washed in HBSS, incubated with 0.25% trypsin/EDTA for 7 minutes at 37°C and the digestion is blocked with DMEM High Glucose (in 10% FBS in with 1% Penicillin/Streptomycin and 1% L-glutamine). Then, cortices are accurately washed and mechanically

dissociated by pipetting in neuron culture medium (Neurobasal plus, 2% B27 plus, 1% Penicillin/Streptomycin). Cell count is performed with an automated cell counter by using Trypan blue (Countess Automated Cell Counter, ThermoFisher). Depending on experimental needs, neurons are seeded on poly-D-lysine (0.1 mg/mL)-coated plates or poly-D-lysine-coated glass coverslips.

3.2.2 Primary cultures of cortical astrocytes

Primary astrocyte cultures are prepared from cerebral tissue of P0-P3 WT and *Mecp2* KO mice. Mice are decapitated and brain is removed. Meninges are carefully removed and cortices are isolated and immersed in HBSS containing 10 mM HEPES and 4 mM $NaHCO_3$. Tissues are then incubated in 0.25% trypsin/EDTA for 30 minutes at 37°C, mechanically dissociated in astrocyte culture medium (DMEM high glucose, Ham F-10 Nutrient Mix, 10% FBS, 1% penicillin/streptomycin) and filtered through cell strainers of 40 µm pore size to obtain a single cell suspension. The resulting cells are centrifuged at 1,500 g for 7 minutes, resuspended in culture medium, and plated in poly-D-lysine (15 µg/mL)-coated 75 cm^2 flasks. At DIV4, flasks are shacked in astrocyte culture medium containing 10 mM HEPES at 200 rpm for 6 hours at 37°C to eliminate residual microglia, and the medium is replaced with fresh culture medium. Cells are incubated in a humidified incubator at 37°C and 5% CO2 and culture medium is refreshed every 4 days. When astrocytes reached confluence (DIV12-DIV15), they are detached by 0.25% trypsin/EDTA diluted 1:3 in HBSS and counted in Countess Automated Cell Counter. Depending on experimental needs, they are seeded on poly-D-lysine (15 µg/mL)-coated plates, poly-D-lysine (1 mg/mL)-coated glass coverslips or transwell membrane inserts (pore diameter 0.4 µm).

3.2.3 Astrocyte-neuron co-cultures

In contact co-culture

Astrocytes (30,000 cells) are plated on glass coverslips and after 2–4 days, neurons are added on the top of astrocyte monolayers at low density (10,000 cells/well). Cells are cultured, during the first 48h, in a 5% FBS co-culture medium (Neurobasal plus medium containing 5% FBS, 2% B27, 1% P/S), then in a medium containing lower serum concentration (Neurobasal medium containing 2.5% FBS, 2% B27, 1% L-

Glutamine, 1% P/S) for the entire duration of the experiment, corresponding to 14 days for neurons. Co-cultures are filled with fresh medium at DIV7 for a third of the original volume.

Transwell-based co-culture

Astrocytes are seeded in astrocyte culture medium on PET membrane cell culture inserts (pore diameter 0.4 µm) at a density of 8,000 cells/insert for 24-well dishes and 150,000 for 6-well dishes. After 4 days, neurons are seeded in neuron culture medium, respectively on PDL coated coverslips in 24-well dishes at a density of 25,000 cells/well on glass coverslips or in 6-well dishes at a density of 200,000 cells/well. After neurons attached to coverslips or wells (~ 2 hours), inserts with astrocytes are carefully transferred on neuron-containing plates and maintained for the entire duration of the experiment in neuronal medium. Cultures are filled with fresh medium at DIV7 for a third of the original volume.

3.2.4 Collection of astrocyte conditioned medium (ACM) or co-culture conditioned medium (CCM)

Astrocytes are seeded in 6-well dishes at a density of 100,000 cells/well. When confluence is reached, astrocyte culture medium is replaced by serum-free medium for conditioning. In details, after a rapid wash to remove cell debris and serum-containing medium (Neurobasal plus, 1% Penicillin/Streptomycin), cells are incubated in 2 mL/well of serum-free medium for 1 hour and 30 minutes. Then, ACM is collected after 48 hours and immediately centrifuged at 1,200 rpm for 5 minutes at 4 °C to remove cellular debris. Protease inhibitor is added to supernatant (1:1,000) and samples are stored at -80°C.

Co-culture conditioned medium (CCM) is collected after 14 days of co-culture between astrocytes on transwells and plated neurons. Protease inhibitor (1:1,000) is added to samples that are stored at -80°C.

Materials

- Hanks' balanced salt solution (HBSS), SIGMA, cod. H6648
- Trypsin-EDTA (0,25%) phenol red, ThermoFisher, cod. 25200-056
- Dulbecco's Modified Eagle's Medium (DMEM), high glucose, pyruvate, ThermoFisher, cod. 41966029

- Ham's F-10 Nutrient mix, ThermoFisher, cod. 31550023
- Neurobasal plus medium, ThermoFisher, cod. A3582901
- L-Glutamine solution, ThermoFisher, cod. G7513
- Penicillin-Streptomycin, ThermoFisher, cod. P0781
- B27 Supplement plus (50X), ThermoFisher, cod. A3582801
- Fetal Bovine Serum (FBS), qualified, heat inactivated, E.U.-approved, South America Origin, GIBCO (ThermoFisher), cod. 10500064 GIBCO
- Cell strainers, 40 µm, Falcon, cod. 352340
- Poly-D-lysine hydrobromide 100MG, SIGMA, cod. P7886
- Coverslips PDL coated, NEUVITRO, cod. GG-12-PDL
- HEPES solution 1 M, pH 7.0-7.6, sterile-filtered, SIGMA, cod. H0887
- Protease Inhibitor Cocktail, SIGMA, cod. P8340
- Falcon® Permeable Support for 6-well Plate with 0.4 µm Transparent PET Membrane, CORNING, cod. 353090
- ThinCert™ Cell Culture Inserts 24 Well plates, tc, sterile, translucent membrane (PET), pore diameter: 0,4 µm, Greiner Bio-One, cod. 662640

3.3 MACS sorting

Astrocytes are isolated from P7 *Mecp2* KO, HET and WT mice to perform gene expression analysis. Cortex isolation from both hemispheres is performed after careful removal of skin, cartilage and meninges and tissues are maintained in HBSS supplemented with 10 mM HEPES
, 4 mM $NaHCO_3$ and 1% P/S until processing. Samples dissociation is obtained both enzymatically by incubation for 5 minutes at 37°C in 0.05% trypsin/EDTA containing DNase I (1:1,000) and mechanically, by gently pipetting. Then cell suspension is filtered through 40µm pore size cell strainers and two volumes of astrocyte culture medium are added. After 1,000 rpm centrifugation for 10 minutes at 4°C, samples are incubated with biotin-conjugated anti-ACSA1 antibody, for selective isolation of astrocytes. The subsequent addition of streptavidin-coated magnetic beads resulted in magnetic labelling of ACSA1-positive cells, which are retained on ferromagnetic columns placed in a magnetic field. After cells collection, 1 mL of PureZOL is added to each sample and cell lysates are stored at -80°C until RNA extraction.

Materials

- Hanks' balanced salt solution (HBSS), SIGMA, cod. H6648
- HEPES solution 1 M, pH 7.0-7.6, sterile-filtered, SIGMA, cod. H0887
- Trypsin-EDTA (0,25%) phenol red, ThermoFisher, cod. 25200-056
- Biotin-conjugated anti-ACSA1 antibody MicroBead Kit, Miltenyi Biotec cod. 130-095-826
- MS columns, Miltenyi Biotec, cod. 130-042-201
- Magnetic Separator, Miltenyi Biotec, cod. 130–042-302
- Cell strainers, 40 µm, Falcon, cod. 352340
- DNase I Amplification Grade, SIGMA, cod. AMPD1
- PureZOL, Bio-rad, cod. 7326890

3.4 Treatments on cell culture

3.4.1 Treatment of neurons with ACM/CCM

Collected ACM/CCM is heated at 37°C in a water bath and added to neurons (1:1 respect to neuron culture medium) for 24 hours from DIV13 to DIV14.

3.4.2 Treatment of neurons with recombinant IL-6

WT cortical neurons (30,000 cells/coverslip) are treated with recombinant IL-6 (200 pg/mL) every 2 days, starting from DIV2. Untreated neurons are filled with an equal volume of culture medium. Neurons are analyzed at DIV14.

3.4.3 Treatment of co-cultures with the neutralizing anti-IL6 antibody

Transwell-based co-cultures are treated with either neutralizing antibody for IL-6 (0.5 mg/mL) or an isotypic antibody Rat IgG_1 (1 mg/mL), diluted 1:500 and 1:1,000, respectively, in the final volume of culture medium (Neurobasal containing 2% B27, 1% L-Glutamine, 1% P/S). Treatment is performed at DIV5 for dendritic length analysis and at DIV5 and DIV12 for synaptic puncta analyses. Untreated co-cultures are filled

with an equal volume of culture medium. In addition, at DIV5, transwell inserts are filled with either 50 µL (when in 24-well plates) or 100 µL (when in 6-well plates) of medium.

3.4.4 Trofinetide treatment on astrocytes

Astrocytes are seeded in 6-well dishes at a density of 100,000 cells/well. When confluence is reached, astrocyte culture medium is replaced by serum-free medium and Trofinetide at a final concentration of 50 µg/mL is added for 72 hours. Untreated cells are supplemented with an equal volume of serum-free medium.

3.4.5 Cholesterol supplementation

WT neurons are treated with either WT or KO ACM at DIV13 for 24h. Immediately after ACM addition, water-soluble cholesterol powder is dissolved in neuron culture medium at a final concentration of 0.1 µg/mL. For WT and HET neurons the same dose of cholesterol is directly added in each well at DIV13, with no ACM treatment. For both experimental settings, untreated cells are supplemented with an equal volume of neuronal culture medium.

Materials

- Recombinant Murine Interleukin-6, Peprotech, cod. 216-16
- Rat monoclonal IgG1 anti-IL6 antibody, R&D Systems, cod. MAB406,
- Water soluble cholesterol, Sigma-Merck, cod. C4951
- Rat IgG1, kappa Isotype Control, Unconjugated, BD Bioscience, cod. 554682
- Trofinetide 10mg, HY-16757, MedChemExpress (MCE)

3.5 Immunofluorescence

3.5.1 Immunofluorescence for neuronal morphology and synaptic puncta analysis

Cell fixation

Neurons (DIV 7 or DIV14) are fixed for 8 minutes with 4% paraformaldehyde dissolved in PBS1X (137mM NaCl, 2.7mM KCl, 10mM Na_2HPO_4, 1.8mM KH_2PO_4) with 10%

sucrose, then washed three times with PBS1X and stored in PBS1X-sodium azide 0.1% at 4°C.

Immunostaining for neuronal dendrites and synaptic markers

After a wash in PBS1X to remove sodium azide, cells are permeabilized in PBS1X – Triton X-100 0.2% for 3 minutes on ice. Then, cells are washed in PBS1X – BSA 0.2% and blocked in PBS1X – BSA 4% for 15 minutes. Incubation with primary antibodies in incubation solution (PBS1X – BSA 0.2%) is performed overnight at 4°C.

The following primary antibodies are used: rabbit anti-Map2 (1:1,000), chicken anti-Synapsin1/2 (1:500), mouse anti-Shank2 (1:300). After washing in PBS1X – BSA 0.2%, cells are incubated with the specific Alexa Fluor 488/568/647 secondary antibodies (1:500) in PBS1X – BSA 0.2% for 1 hour in the dark. Cells are washed 5 times in incubation solution. Nuclei are stained with DAPI solution (1:1,000 in PBS1X) following a 10 minutes incubation and cells are washed in PBS1X. After a last wash in water, glass coverslips are mounted on microscope slides with Fluoromount Aqueous Mounting Medium and stored at 4°C until image acquisition.

3.5.2 Immunofluorescence for astrocyte marker GFAP

Cell fixation

To assess the efficiency of MACS sorting, 10 µL cell suspension is transferred on glass coverslips. Astrocytes are fixed for 8 minutes with 4% paraformaldehyde dissolved in PBS1X then washed three times with PBS1X and stored in PBS1X-sodium azide 0.1% at 4°C.

Immunostaining for the astrocytic marker Gfap

Cells are washed in PBS1X and then permeabilized in PBS1X containing 0.2% Triton X-100 for 3 minutes on ice. After three washes in PBS1X containing 0.2% BSA, blocking solution (4% BSA in PBS1X) is added for 15 minutes before incubating the primary antibodies (Gfap, 1:500), diluted in PBS1X containing 0.2% BSA overnight (4°C). Then, cells are washed in PBS1X containing 0.2% BSA before the incubation with Alexa Fluor secondary antibodies for 1h at RT. Antibodies are diluted 1:500 in PBS1X containing 0.2% BSA. Several washes in 0.2% BSA in PBS1X are then performed and nuclei are stained with 1:1,000 DAPI in PBS1X solution for 10 minutes

at RT. Finally, cells are washed in PBS1X before mounting the coverslips on glass microscope slides with Fluoromount Aqueous Mounting Medium.

Materials

- 2,2,2-Tribromoethanol, SIGMA, cod. T48402
- Bovine Serum Albumin (BSA), SIGMA, cod. A3059
- Horse serum, SIGMA, cod. H0146
- Coverslips 24 x 50 mm, Menzel-Glaser
- DAPI Solution (1 mg/mL), ThermoFisher, cod. 62248
- Fluoromount Aqueous Mounting Medium, SIGMA, cod. F4680
- Microscope slides, Thermo Scientific, cod. AFAA000001##12E
- *n*-Pentane 99% RE, Carlo Erba, cod. 528993
- 16% Paraformaldehyde (Formaldehyde) Aqueous Solution, EM Grade, Electron Microscopy Science (SIC), cod. 15700-1L
- PolyFreeze Tissue Freezing Medium, SIGMA, cod. SHH0026
- Potassium phosphate monobasic, SIGMA, cod. V000225
- Sodium azide, SIGMA, cod. S2002
- Sodium chloride, SIGMA, S9888
- Sodium hydroxide, SIGMA, cod. 221465
- Sodium azide, SIGMA, cod. S2002
- Sucrose, SIGMA, cod. S9378
- Triton X-100, SIGMA, cod. T8787

Antibodies

- Gfap cloneGA5, Merck Millipore, Mouse, cod. MAB 3402
- Map2 (D5G1), Cell Signaling, Rabbit, cod. 8707
- Shank2, Synaptic Systems, Mouse, cod. 162211
- Synapsin1/2, Synaptic Systems, Chicken, cod. 106006
- Donkey anti-Mouse IgG (H+L) Highly Cross-Adsorbed Secondary Antibody, Alexa Fluor 488, ThermoFisher, cod. A21202
- Donkey anti-Mouse IgG (H+L) Highly Cross-Adsorbed Secondary Antibody, Alexa Fluor 568, ThermoFisher, cod. A10037

- Donkey anti-Rabbit IgG (H+L) Highly Cross-Adsorbed Secondary Antibody, Alexa Fluor 647, ThermoFisher, cod. A31573
- Goat anti-Chicken IgG (H+L), Secondary Antibody, Alexa Fluor 488, ThermoFisher, cod.A32931
- Goat anti-Rabbit IgG (H+L) Secondary Antibody, Alexa Fluor 568, ThermoFisher, cod. A11036
- Goat anti-Guinea pig igG (H+L) Secondary Antibody, Alexa Fluor 488, Thermofisher, cod. **A11073**

3.6 Microscopy and image analysis

3.6.1 Total dendritic length

To analyze the total dendritic length, images of WT neurons (at DIV6) are acquired at Nikon Eclipse Ti at 20X. Dendritic length is evaluated using NeuronJ, a plugin of ImageJ, by measuring the length of each dendrite for each neuron and calculating the sum of such values, corresponding to the total dendritic length.

3.6.2 Synaptic puncta on neuronal cultures

To analyze synaptic markers, z-stack images of synaptic puncta (1,024X1,024 pixel resolution) are acquired at 1.43 digital zoom using a 63X oil-immersion objective mounted on a Leica DMI3000B microscope equipped with an Sp5 laser-scanning confocal system (8-bit grayscale depth images). Acquisition of synaptic puncta is performed using a step size of 0.30 μm. By Fiji software, maximum intensity projection images are converted to binary images and processed with a fixed threshold for each channel acquired. Puncta density is calculated by counting only puncta lying along manually selected ROIs within 20 μm of 3 primary branches/neuron. Only puncta with a minimum size of 0.16 μm^2 are counted using Analyze Particles. To assess puncta colocalization of pre- and post-synaptic markers, the Fiji Plugin Colocalization highlighter is run on each z-stack image acquired. Colocalized puncta are quantified in manually selected ROIs of the binary mask created from the maximum intensity projection. Only puncta with a minimum size of 0.1 μm^2 are counted.

3.7 Gene expression analysis

3.7.1 RNA extraction

Total RNA is extracted from neurons cultured in 6-well plates, from astrocytes cultured in 6-well plate, from astrocytes cultured on 6-well transwell inserts and from astrocytes sorted from P7 mouse cortices. RNA is also extracted from HET and WT mouse brain areas at the established post-natal day. Cells or tissues are lysed in the appropriate volume of PureZOL. For brain areas collection, mice are sacrificed by dislocation and brains are rapidly removed. Selected tissues (cortex, hippocampus and cerebellum) are dissected and immediately frozen on dry-ice and stored at -80°C until analysis.
Both for cells and tissues, chloroform 1:5 is added, followed by manual inversion of sample and centrifugation at 12,000 g for 15 minutes at 4°C. After collection of the aqueous phase, isopropanol 1:1 (considering PureZOL volume) containing 10 µg glycogen RNA grade is added to the samples, to allow overnight precipitation at -20°C. The day after, samples are centrifuged at 12,000 g for 10 minutes at 4°C and the obtained RNA pellet is centrifuged again at 7,500 g for 10 minutes at 4°C, after a wash in 70% ethanol. Then, for astrocytes isolated by MACS sorting, sample pellets are suspended in RNAse-free H_2O and stored at -80°C. From cells cultured in 6-well plate, RNA pellet is treated with DNase at 37°C for 15 minutes to remove eventual genomic DNA contaminations. Then, enzymatic reaction is inactivated in PureZOL and a second RNA extraction is performed.

3.7.2 RNA quantification and integrity assessment

Extracted RNA is quantified using the spectrophotometer (NanoDrop 1000) and its quality is determined by electrophoresis. In detail, samples are loaded on a gel composed of 1% agarose in TAE1X buffer with the addition of SYBR safe 1:20,000. After a 20-minutes run at 80 V, bands are visualized using an UV transilluminator (Essential V6 system, UVITEC Ltd, UK). RNA integrity is assessed estimating the relative abundance of the three bands corresponding to 28S, 18S and 5S of mouse ribosomal RNA.

3.7.3 Quantitative Reverse Transcription PCR

cDNA is synthesized using the RT^2 First Strand Kit according to the manufacturer's instructions and used as template for qRT-PCR with SYBR Green Master Mix and a QuantStudio 5 Real-Time PCR System (ThermoFisher Scientific). Due to the low amount of RNA extracted from MACS sorted astrocytes, a preamplification step is performed using SsoAdvanced PreAmp Supermix prior to qRT-PCR, following manufacturer's instructions. Melting curve showed a single product peak, indicating good product specificity. The best housekeeping gene is selected for each comparison among *Cyclophilin A*, *Rpl13, Hprt* and *Ywhaz*, and fold change in gene expression is calculated using the 2^(-Delta Ct) method.

Materials

- PureZOL RNA isolation Reagent, Bio-Rad, cod. 7326890
- Chloroform, SIGMA, cod. 372978
- 2-Propanol, SIGMA, cod. 33539
- Ethanol, SIGMA, cod. 32221
- Nuclease-Free Water, SIGMA, cod. W4502
- DNase I Amplification Grade, SIGMA, cod. AMPD1
- RT^2 First Strand Kit, QIAGEN, cod. 33040
- SYBR™ Green PCR Master Mix, Applied Biosystems, cod. 4309155
- SsoAdvanced PreAmp Supermix, Bio-Rad, cod. **1725160**

Primers for tested genes are listed below:

Gene	Forward primer (5'-3')	Reverse primer (5'-3')
Abca1	GTTGCTGTGGATGGCTTG	GGAAACAGCCCAGTCAGT
Abcg1	GACTTGTCTCCACTGCCG	GTCCACTGACACGCACAC
ApoE	CGTGCTGTTGGTCACATTGC	CAGGGTTGGTTGCTTTGCC
C3	GAGTGGGGCTAGTGGCTGTGGA	CCTGGGGTGCAGCCAATGTCTG
C4b	TGGCTCCTTCCACGACCCATGT	AGGGCAATGACCACAAAGGCGG
Ccl2	GCCTGCTGTTCACAGTTGC	ATTGGGATCATCTTGCTGGT
Ccn2	CTTCTGCGATTTCGGCTCCCCC	ACACCGACCCACCGAAGACAC

Cxcl12	TGCATCAGTGACGGTAAACCA	TTCTTCAGCCGTGCAACAATC
Efnb1	AGCCACACCAGGAAATCCGC	CGGTTCTCCAGTCCCTCCAA
Hmgb1	GCAGCAGATGACAAGCAGCCCT	TGACCACCCCCTTTTTCGCTGC
Hmgcr	CCTACGGCAGCTTGGGTCC	GCCTGTCAGTTCTTTGTCG
Hprt	ACAGGCCAGACTTTGTTGGAT	TGCAGATTCAACTTGCGCTC
IL-17r	CACCCCAAAAACCTGACCCCG	TGACACACAGCCGCTCATTGG
IL-1β	AGTTGACGGACCCCAAAAGA	GGACAGCCCAGGTCAAAGG
IL-33	GCAAAGTTCAGCAGCACCGCAG	AGGCCAGAACGGAGTCTCATGCA
IL-6	CGGAGAGGAGACTTCACA	AGAATTGCCATTGCACAAC
Lcat	AGATCCGTGTCCCTGGCT	CGCACTGTCTCATCCCGCA
Mecp2	AAACCACCTAAGAAGCCCAAATC	TTGACAACAAGTTTCCCAGGG
Mvk	CCAACACCAAGGTCCCGC	CGTCAATGGAGGTCAGCAG
Nsdhl	GGCGACCTGTGCAACCAACAG	TTACTGTACGGCGGAGGGGACG
Rpl13	TGGCTGGCATCCACAAGAAA	TTCTTCAGCAGAACTGTCTCCC
Sqle	CGTTTCTTCCCACTTCGTTG	GGGTTGACCAGAACAAGCTCCG
Tgfβ	GGAGAGCCCTGGATACCAAC	CAACCCAGGTCCTTCCTAAA
Tnfalfα	ATGAAGCCCTGGAGTGCGTG	CTTTGGTGAGGTTTGATCCG
Vegfα	CGAGGTTGCTGCTGGTGATG	TGGGGTGTGTCGGCTGCA

Table 3. List of the genes tested by qRT-PCR and their respective primers.

3.8 Protein extraction and western blotting

3.8.1 Protein extraction and quantification

From astrocytes and neurons:

Cells are washed with warm PBS1X and lysed by a cell scraper in sample buffer containing 2-Mercaptoethanol (1:10 v/v) and sonicated at 30 Hz for 5 seconds. Samples are stored at -20°C until analysis.

From brain cortices:

Mutant mice and WT littermates at the established post-natal day are sacrificed by dislocation and brains are rapidly removed. Selected tissues are dissected and

immediately frozen on dry-ice and stored at -80°C until analysis. Tissues are sonicated for 10 seconds (30 amplitudes) in ice-cold RIPA buffer (100 mM Tris HCl pH 7.5, 300mM NaCl, 10 mM EDTA, 2% NP-40 0.2%, 1% sodium deoxycholate) containing Protein Inhibitor Complex and PhosSTOP1X. Sonication is repeated for two cycles in case of the hippocampus and 4 times for the cerebral cortex. Tissues are then left on ice for 30 minutes and centrifuged at 13,000g for 30 minutes at 4°C. Supernatants are then collected and stored at -20°C until analysis. Protein concentrations are calculated using bicinchoninic acid (BCA) assay kit following manufacturer's procedure.

3.8.2 Western blot

For western blots on astrocytes or neurons collected in sample buffer, after denaturation at 70°C (for preserving phosphorylation) or 95°C for 5 minutes, an equal volume of each sample is resolved on 4–15% Criterion TGX Precast Protein Gels. For western blots on brain areas, the same amount of protein for each extract is added basing on the BCA quantification and sample buffer is used to prepare samples. Before transfer, a TGX Stain-Free gel image is acquired using a UV-transilluminator (ESSENTIAL V6 System, UVITEC Ltd, UK) and used for relative quantification. Proteins are blotted on a nitrocellulose membrane or onto a PVDF membrane using the Trans-blot SD (Bio-Rad) semidry apparatus and Ponceau S staining is used to verify proper protein transfer. Membranes are then incubated at RT for 1 hour in blocking solution (Tris-buffered saline containing 0.5% Tween 20 (TBST) and 5% non-fat milk or 5% BSA) or for 5 minutes in EveryBlot blocking solution before adding primary antibodies at the proper dilution: anti-NF-kB p65 (1:500 in 5% milk-TBST); anti-phospho-Stat3 (1:1,000 in EveryBlot); anti-Stat3 (1:2,500 in in EveryBlot); anti-Gapdh (1:10,000 in 5% milk-TBST); anti-Nsdhl (1:1000 in 5% milk-TBST). After 3 washes in TBST, blots are incubated with the appropriate HRP-conjugated secondary antibody diluted 1:10,000 in 5% milk, 5% BSA-TBST or EveryBlot. Immunocomplexes are visualized using the ECL substrates kits from Cyanagen and imaged on ALLIANCE MINI HD9 system (UVITEC Ltd, UK). Quantification of bands is performed using the Uvitec Nine Alliance Software, with the relative density of bands corrected on background signal. P65 signal is normalized on Gapdh. For the other protein targets, band intensity is normalized on total protein content quantified by using TGX Stain-Free gel.

Materials

- Protein Inhibitor Cocktail (PIC) 1X, Sigma Merck, cod. P8340
- PhosSTOP 1X, Sigma Merck, cod. 4906845001
- Bicinchoninic acid (BCA) assay kit,Thermo Scientific, cod. 23228
- Ethylenediaminetetraacetic acid (EDTA), SIGMA, cod. EDS
- NP-40 (IGEPAL), SIGMA, cod. CA630
- Sodium dodecyl sulfate (SDS), SIGMA, cod. L3771
- Sodium chloride, SIGMA, S9888
- Instant milk, 0% fat, Regilat
- 2-mercaptoethanol, SIGMA, cod. M6250
- Bovine Serum Albumin (BSA), SIGMA, cod. A7906-100G
- Criterion TGX Stain-free Protein gel, Bio-Rad, cod. 5678085, 5678084
- Laemmli 4X sample buffer, BioRad, cod. 1610747
- Trans-blot Turbo Midi Nitrocellulose Transfer Packs, Bio-Rad, cod. 1704159
- Trans-Blot Turbo Midi 0.2 µm PVDF Transfer Packs, Bio-Rad, cod. 1704157
- Ponceau S, SIGMA, cod. P3504
- Tween 20 500 mL, SIGMA, cod. P1379
- EveryBlot Blocking Buffer, Bio-Rad, cod. 12010020
- WESTAR ANTARES, Cyanagen, cod. XLS1420250
- WESTAR SUN, Cyanagen, cod. XLS0630250
- WESTAR SUPERNOVA, Cyanagen, cod. XLS30100

Antibodies

- Phospho-Stat3 (Tyr705) (D3A7) XP®, Cell Signaling, Rabbit, cod. 9145
- Stat3 (124H6) antibody, Cell Signaling, Mouse, cod. 9139
- NF-kB p65 (F-6), Santa Cruz, Mouse, cod. sc-8008
- Gapdh, Invitrogen, Rabbit, cod. MA1-16757
- Nsdhl (D-11), Santa Cruz, Mouse, cod. 390871
- HRP conjugate Goat polyclonal anti-mouse, Jackson ImmunoResearch, cod. 115-035-003
- HRP conjugate Goat polyclonal anti-mouse, Jackson ImmunoResearch, cod. 111-035-144

3.9 Cytokines quantification

Cytokines are detected in CCM by FRACTAL Unit (Flow cytometry Resource, Advanced Cytometry Technical Applications Laboratory, San Raffaele Scientific Institute, Milan) with two LEGENDplex assay kits: LEGENDplex Mouse Cytokine Release Syndrome Panel and LEGENDplex Mouse Cytokine Panel 2 according to the manufacturer's instructions. Cell culture media are used undiluted. Samples are acquired using a BD FACSCantoTM II Cell Analyzer (BD Biosciences) using BD FACS Diva software and equipped with three lasers: blue (488 nm), red (633 nm) and violet (405nm). FCS files are analyzed by using LEGENDplex Data Analysis Software (BioLegend) according to the manufacturer's instructions, obtaining the absolute concentration for each molecule.

Materials

- LEGENDplex Mouse Cytokine Release Syndrome Panel, Biolegend, cod. 741023
- LEGENDplex Mouse Cytokine Panel 2, Biolegend, cod. 740134

3.10 ELISA assay for IL-6

KO astrocytes, plated on transwell inserts, are maintained in cultures with WT neurons for 14 days (corresponding to neurons DIV14). At this time point, astrocytes are transferred into new plates with the original medium but in the absence of neurons, and maintained in cultures for other 8 days. Immediately after neuronal removal and 4 and 8 days later, an aliquot of medium is collected from each well and frozen at 80°C, in the presence of protease inhibitor (1:1000). By ELISA assay, IL-6 concentration is quantified according to the manufacturer's instruction. IL-6 concentration is also calculated in KO ACM.

Materials

- ELISA assay, Immunological Sciences, cod. IK4209

3.11 MTT assay

For MTT assay, WT cortical neurons are seeded in a 96-wells plate at a density of 10.000 cells/well. At DIV13 the cells are treated with increasing concentrations of cholesterol, deduced from literature (161,162). As control, neuronal cells are treated with an equal volume of neuronal medium. 24 hours after treatment, neurons are incubated for 4 hours with a solution of 4 mg/mL MTT (Sigma-Aldrich) in PBS1X, properly diluted in neuronal medium. Then the medium is removed and 100µl dimethyl sulfoxide (DMSO) is added in each well. Cell viability is assessed through spectrophotometer (Victor^2, Wallac, 1420 multilabel counter) lecture of the plate at 450 nm and comparing untreated cells values with treated ones.

Materials

- Cell proliferation kit (MTT), Sigma-Aldrich, cod. 11465007001
- Dimethyl sulfoxide (DMSO), SIGMA, cod. D8418

3.12 Statistical analysis

All statistical analyses are performed using Prism 10 (GraphPad Software, LLC). Data are expressed as mean ± SEM, except for violin plots in which the bar indicates the median with interquartile range. Number of biological or technical replicates are indicated in figure legends. Grubbs' test is performed to identify outliers. Comparisons between two groups is performed by Student's t-test or Mann-Whitney test according to data distribution. Instead, multiple groups' comparisons are performed through two-way ANOVA, followed by Tukey's or Sidak's post hoc tests. A p-value <0.05 is considered significant: *$p<0.05$, **$p<0.01$, ***$p<0.001$, ****$p<0.0001$.

4. Results

4.1 Preliminary data

4.1.1 Factors released by *Mecp2* knock-out (KO) astrocytes are detrimental for synapse development and maintenance

As mentioned in the introduction, many researchers depicted the negative influence of *MECP2* mutant astrocytes on neuronal development and functioning (103,104,151). Since many functions of astrocytes are exploited through the release of gliotransmitters, proteomic and metabolomic analyses of astrocyte conditioned medium (ACM) collected from *MECP2* mutant astrocytes unveiled a plethora of differentially expressed molecules, which could be responsible for the observed detrimental effects on neurons (93,156,163). Although these studies have been fundamental to gain insight into the alterations of secretome composition directly related to *Mecp2* deficiency, they exclusively focused on astrocytes cultured alone, without considering the crosstalk with neurons, which strongly affects molecular and functional properties of both cell populations (106,109,164). In this context, our laboratory is particularly interested in unveiling the impact of non cell-autonomous effects elicited by *Mecp2* knock-out (KO) astrocytes on the synaptic phenotype, that is known to be strongly impaired in RTT brain (42,82,83). For this purpose, we exploited two different *in vitro* culture systems. On one hand, to consider the factors secreted by astrocytes only in dependence of their genotype, we treated neurons with ACM collected from mono-cultures of either wild type (WT) or KO astrocytes. On the other hand, we exploited a co-culture system between neurons and astrocytes, in which the latters are cultured on transwell inserts which prevent the direct contact with neurons while allowing the exchange of secreted molecules. This setting enables the exploration of the crosstalk between astrocytes and neurons in a more physiological and comprehensive manner. Interestingly, by using the two different approaches, we observed that both KO astrocytes and their ACM induced synaptic defects in WT neurons. Going in details, in the first experimental setting, we treated WT neurons for 24 hours (from DIV13 to DIV14) with WT and KO ACM and, to analyze the synaptic phenotype, we performed immunofluorescence staining for pre-synaptic (Synapsin1/2) and post-synaptic (Shank2) proteins (Figure 7A). We unveiled that the treatment with KO ACM, compared to the treatment with WT ACM, causes a significant reduction in

the number of pre- and post-synaptic markers, ultimately leading to a consistent reduction of synaptic proteins colocalization, which is considered an index of active synapses. Interestingly, heating KO ACM at 95°C (KO ACM*) prevents its detrimental effect on synapses, demonstrating the thermolabile nature of synaptotoxic factors (Figure 7B-7E).

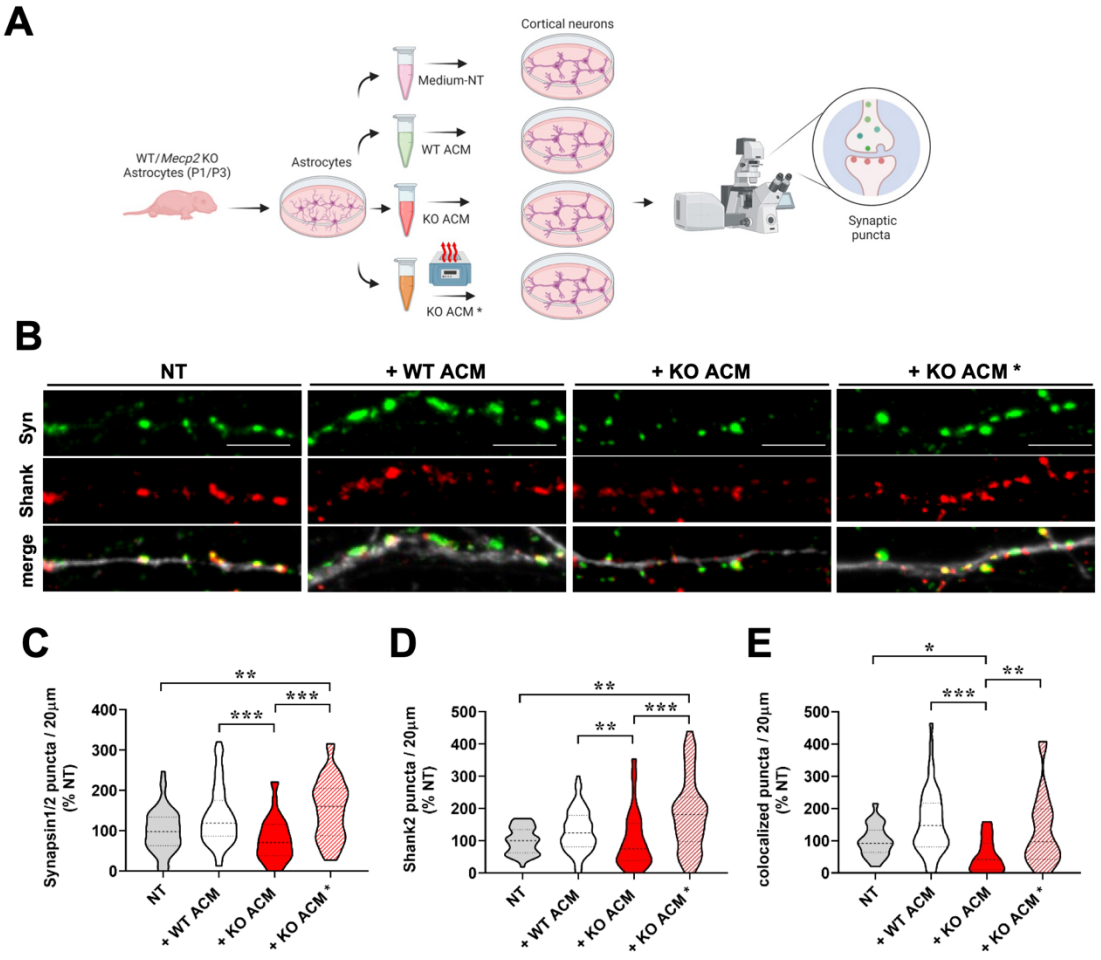

Figure 7. Treatment of WT neurons with KO ACM impairs synaptic phenotype. (A) Astrocyte conditioned medium (ACM) is collected from *Mecp2* KO or WT astrocytes in mono-cultures. WT neurons are left untreated (NT) or treated with either WT, KO ACM or KO ACM* (heat inactivated ACM). (B) Representative images of synaptic proteins Synapsin1/2 (green) and Shank2 (red) on selected primary dendrites of neurons treated with WT ACM, KO ACM, KO ACM* or left untreated (NT). Scale bar = 5 µm. (C-E) Violin plots represent the median (dashed lines) and 25th and 75th percentiles (dotted lines) of the number of Synapsin1/2 (C) and Shank2 puncta (D) and their colocalization (E). For all the graphs, data are expressed as percentages and compared to NT neurons (set at 100%). Statistical analysis is performed by Kruskal Wallis test, followed by Dunn's post-hoc test (*p<0.05, **p<0.01, ***p<0.001). The

number of neurons analyzed for each experimental group is >24, from at least 3 biological replicates. Samples derive from 2 independent experiments.

To further study synaptic phenotype in a more physiological condition, including the bidirectional communication between astrocytes and neurons, we moved to the transwell based co-culture system. In details, either WT or KO cortical astrocytes were cultured on transwell inserts and transferred above WT cortical neurons for 14 days (Figure 8A). Subsequently, immunofluorescence staining performed on the pre- and post-synaptic proteins revealed a significant decrease in the density of both synaptic markers in neurons exposed to paracrine factors secreted by KO astrocytes (Figure 8B-8C). Moreover, when in culture with RTT astrocytes, WT neurons also showed a strong reduction of the colocalization of Synapsin1/2 and Shank2 puncta (Figure 8D). Importantly, the same results were obtained in co-cultures in which WT neurons and KO astrocytes were maintained in contact, thus revealing the strong contribution of secreted molecules in the arise of synaptic defect in RTT (Figure 8F). However, the area of Synapsin1/2 puncta appears significantly reduced in contact co-cultures, while it is not affected when neurons are only exposed to paracrine signals, underlining the role of direct interactions between neurons and astrocytes in shaping the synapse structure (Figure 8E-8G).

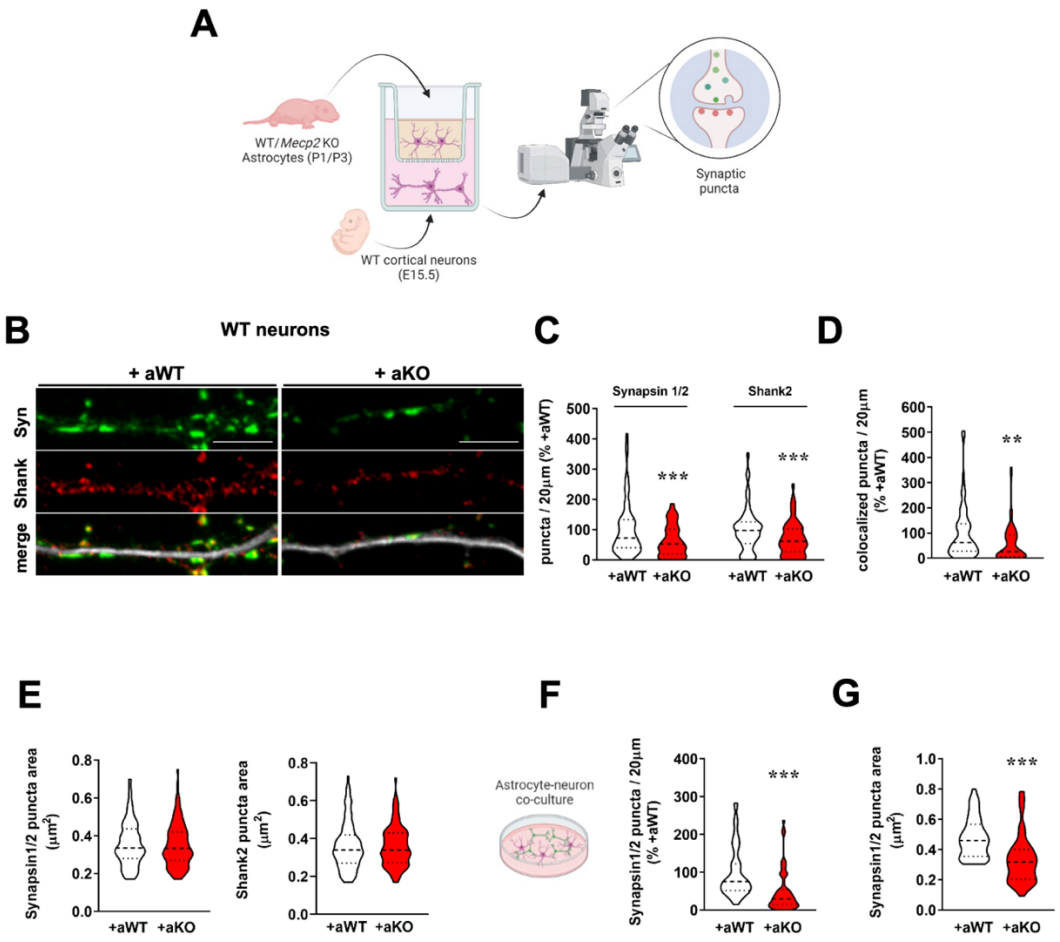

Figure 8. WT neurons cultured with KO astrocytes show impaired synapse formation. (A) Astrocytes obtained from KO or WT pups are cultured on transwell inserts and transferred on WT neurons at DIV0. After 14 days of co-culture, immunofluorescence staining for synaptic proteins is performed. (B) Representative images of synaptic proteins Synapsin1/2 (green) and Shank2 (red) puncta on selected primary dendrites of neurons exposed either to WT astrocytes (+aWT) or to KO astrocytes (+aKO). Scale bar = 5 µm. (C,D,F) Violin plots represent the median (dashed lines) and 25th and 75th percentiles (dotted lines) of the number of Synapsin1/2 (C,F) and Shank2 (C) puncta and their colocalization (D). For described graphs, values for puncta number and colocalization are expressed as percentages compared to +aWT co-cultures (set at 100%). (E,G) Violin plots display the absolute values of the areas of Synapsin1/2 or Shank2 puncta (µm^2) in +aWT and +aKO transwell based co-cultures (E) and in contact co-cultures (G). For all the graphs, Student's t-test or Mann-Whitney test were applied according to data distribution for statistical analysis (**p<0.01, ***p<0.001). The number of neurons analyzed for each experimental group is >50, from at least 3 biological replicates and data are obtained from at least 2 independent experiments.

4.1.2 Transcriptional analysis in neurons confirms the negative impact of Mecp2 KO astrocytes on synaptic phenotype, unveiling the involvement of inflammatory molecules.

The observed synaptic defect could result both from the lack of beneficial cues and the production of synaptotoxic factors by *Mecp2* KO astrocytes. To gain insight on the nature of secreted molecules that could impact synapses, we exploited an indirect strategy, focusing on the analysis of gene expression in cortical neurons exposed to either WT or KO astrocytes paracrine cues in the transwell based co-culture system. This approach allowed us to unveil the main affected downstream pathways and deduce upstream molecules. An alternative approach could be proteomic analysis on the co-culture medium, that is methodologically complicated by the interference of high levels of albumin. We thus performed RNA sequencing analysis comparing 3 experimental groups: WT neurons cultured alone (CTRL), with WT astrocytes (+aWT) or with KO astrocytes (+aKO) (Figure 9A). Principal component analysis (PCA) revealed that WT neurons in co-culture with astrocytes, regardless of *Mecp2* expression, similarly cluster if compared to neurons cultured alone, confirming the huge impact of astrocyte signals on neuronal gene expression (Figure 9B). Besides confirming the expected synaptic alterations, bioinformatics analyses highlighted a prominent activation of pathways related to inflammatory response in WT neurons cultured with KO astrocytes (Figure 9E). Based on this evidence, we aimed to better dissect the involvement of inflammatory cues in RTT pathogenesis exploiting different strategies to identify potential targets.

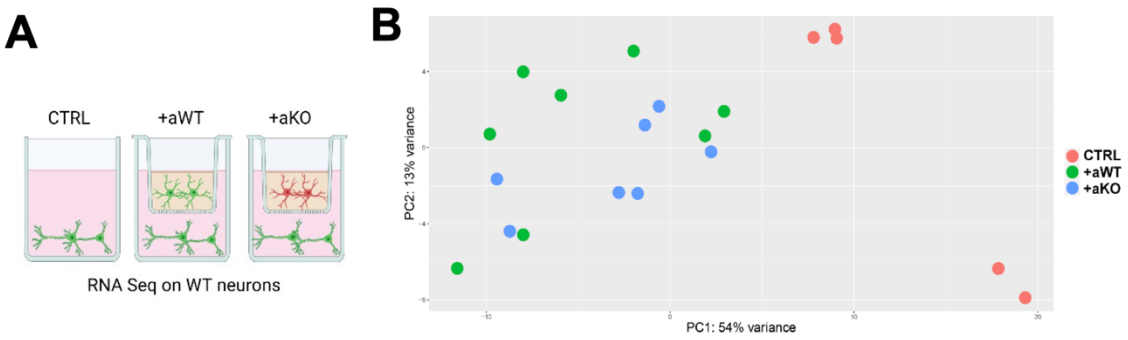

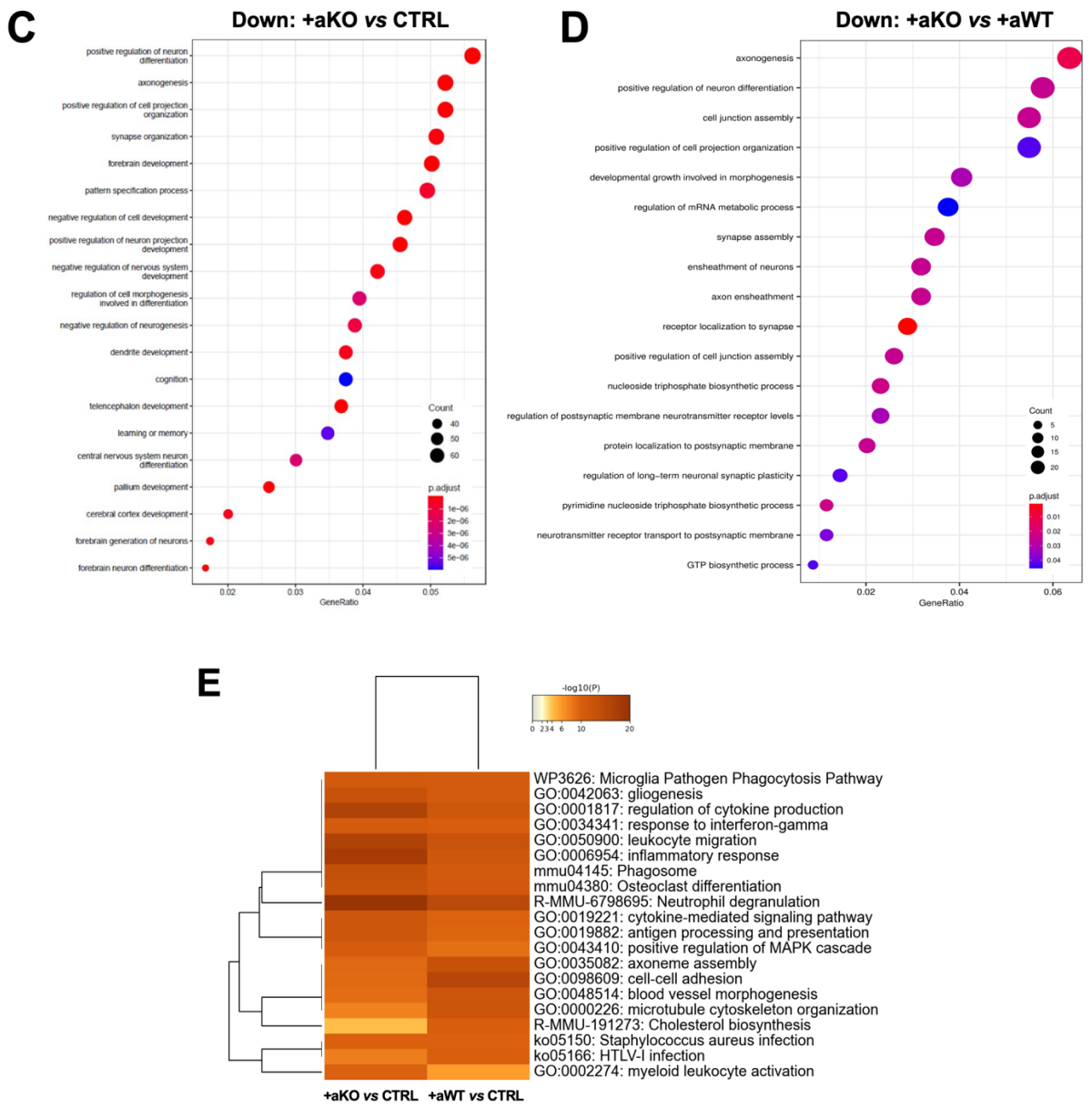

Figure 9. WT neurons exposed to KO astrocytes paracrine cues show a down-regulation of pathways related to synapses and a consistent activation of pathways related to inflammatory response. **(A)** The scheme represents the 3 experimental groups considered for this analysis: WT neurons cultured alone (CTRL) or co-cultured with either WT (+aWT) or *Mecp2* KO (+aKO) astrocytes seeded on transwell inserts for 14 days. **(B)** PCA graph shows the individual sample variances between the 3 experimental groups. Each dot represents a sample. On the axes the percentage of total variation among samples is reported. For CTRL, n=5; for +aWT, n=7, for +aKO, n=8. WT neurons are obtained from a pool derived from 3 different embryos. **(C-D)** Gene Ontology (GO) analysis of +aKO vs CTRL **(C)** and +aKO vs +aWT **(D)** comparisons showing the top 20 enriched GO terms (biological processes) from DEGs with p.adjust <0.05. The dimension of the dots represents the number of genes counted for the corresponding biological process, while the colour intensity indicates the value of the

p.adjust. **(E)** Metascape analysis of up-regulated pathways from the comparison between +aKO vs CTRL vs +aWT vs CTRL. The heatmap shows the biological processes of interest with their -$\log_{10}$ p-value, selected from the 100 enriched terms across the two gene lists.

4.2 *Mecp2* KO astrocytes affect synaptogenesis by Interleukin-6 (IL-6) dependent mechanisms

4.2.1 *Mecp2* KO astrocytes induce the expression of inflammatory-related factors in WT neurons

To validate the increased inflammatory response in WT neurons cultured with KO astrocytes, we first evaluated in neurons the expression of genes associated with the relevant pathways by using qRT-PCR. We unveiled the significant upregulation of a panel of genes related to cytokine signaling in +aKO conditions, including genes coding for transcription factors Stat2 and Stat3 and pathway inhibitors, namely Socs3, Ikbke and Chuk (165,166) (Figure 10A). Further, to prove the increased inflammation induced in WT neurons from KO astrocytes, we analyzed by western blot (WB) the levels of the transcription factor NF-kB (p65) that mediates the expression of many genes involved in inflammatory response (167), finding it significantly upregulated (Figure 10B).

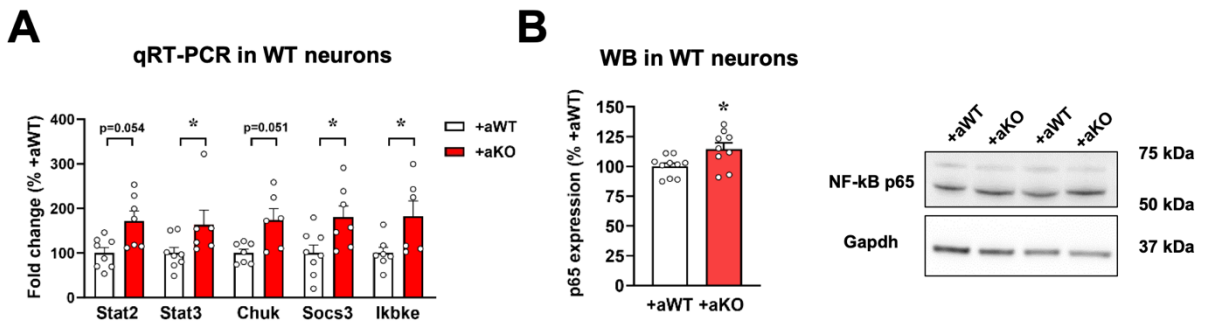

Figure 10. Mecp2 KO astrocytes trigger inflammatory pathways in WT neurons. **(A)** The graph shows the expression level of selected inflammatory-related genes in +aKO compared to +aWT (set at 100%). Data are expressed as mean ± SEM and statistical analyses is performed by Mann-Whitney test (*p<0.05). **(B)** Graph shows the expression level of p65 protein in +aWT (set at 100%) compared to +aKO. Data are expressed as mean ± SEM and

statistical analysis is performed by unpaired Student's t-test (*p<0.05). On the right, representative bands for p65, whose intensity is normalized on Gapdh content.

4.2.2 *Mecp2* KO astrocytes produce excessive levels of IL-6

To verify the activation of inflammatory pathways in KO astrocytes, we measured the transcriptional level of a panel of pro-inflammatory molecules directly in WT and KO astrocytes cultured on transwell inserts. We found a significant increase in the mRNA levels of different cytokines in KO astrocytes, namely *IL-1β*, *IL-6* and *Cxcl12*. Of note, we also observed a significant reduction of *Hmgb1*, a factor that is generally recognized as an inflammation trigger (Figure 11A).

After assessing the inflammatory status induced in WT neurons and the increased cytokines' expression in KO astrocytes, we proceeded to quantify the cytokines and chemokines in the co-culture medium (CCM), by using the Luminex technology (LEGENDplex), a cytometric bead-based immunoassay platform. Obtained results indicated a significant increase in the amount of IL-6 in the CCM of +aKO condition, together with a slight increase of TNFα, CCL2, CCL3 and CCL4. The levels of IL-1β and CXCL12 were not assessed since beads targeting these cytokines were not included in the Luminex assay (Figure 11B).

To verify that astrocytes are actually the primary source of this cytokine, we analysed *IL-6* mRNA levels also in neurons when in co-culture with astrocytes, finding that its expression levels are consistently too low to be detectable by qRT-PCR. We also examined *IL-6* expression in our RNA sequencing data (Figure 9) without finding any changes among the experimental groups, thus indicating that neurons are not significantly contributing to the IL-6 increase.

All in all, these molecular evidence highlighted the excessive secretion of IL-6 in the medium of +aKO condition by *Mecp2* KO astrocytes.

To assess whether IL-6 released by KO astrocytes is active and functional, we analyzed the phosphorylation level of Stat3, the main downstream target of IL-6 (168,169), in neurons treated for 24 hours with the CCM collected from the +aKO and +aWT conditions. Western blot analysis revealed a significantly increase of phospho-Stat3, normalized on the total quantity of Stat3 protein, in neurons treated with +aKO CCM, thus proving that IL-6 released by astrocytes is triggering its downstream pathways in neurons (Figure 11C).

Importantly, considering that the presence of serum in astrocyte cultures could push these cells to acquire a more reactive phenotype (170), we decided to validate our observations in a more physiological condition. Thus, we acutely isolated astrocytes from P7 mice cortices taking advantage of MACS technology that exploits magnetic MicroBeads coupled with antibodies targeting ACSA-2, a membrane marker of neonatal astrocytes. Astrocytes were collected from WT and *Mecp2*$^{+/-}$ female mice (HET) to focus on the mouse model that better represents the mosaicism of affected RTT patients. As first step, we verified the identity of extracted cells after 5 days of culture proving that they were positive for one of the most commonly used astrocyte marker, Glial Fibrillary Acidic Protein (GFAP) (Figure 11D). We proceeded by analyzing the expression level of *IL-6* by qRT-PCR on WT and HET astrocytes, revealing a significant increase of mRNA levels of the cytokine in HET samples (Figure 11E). Interestingly, Pearson's correlation test revealed an inversely proportional correlation between the levels of *Mecp2* and *IL-6* in HET samples: the highest the *Mecp2* expression, the lowest the *IL-6* mRNA levels (Figure 11F). Altogether, these data confirm that astrocytes isolated from both KO and HET cortices produce an excessive amount of IL-6, a cytokine that might contribute to the onset of synaptic defects observed in RTT.

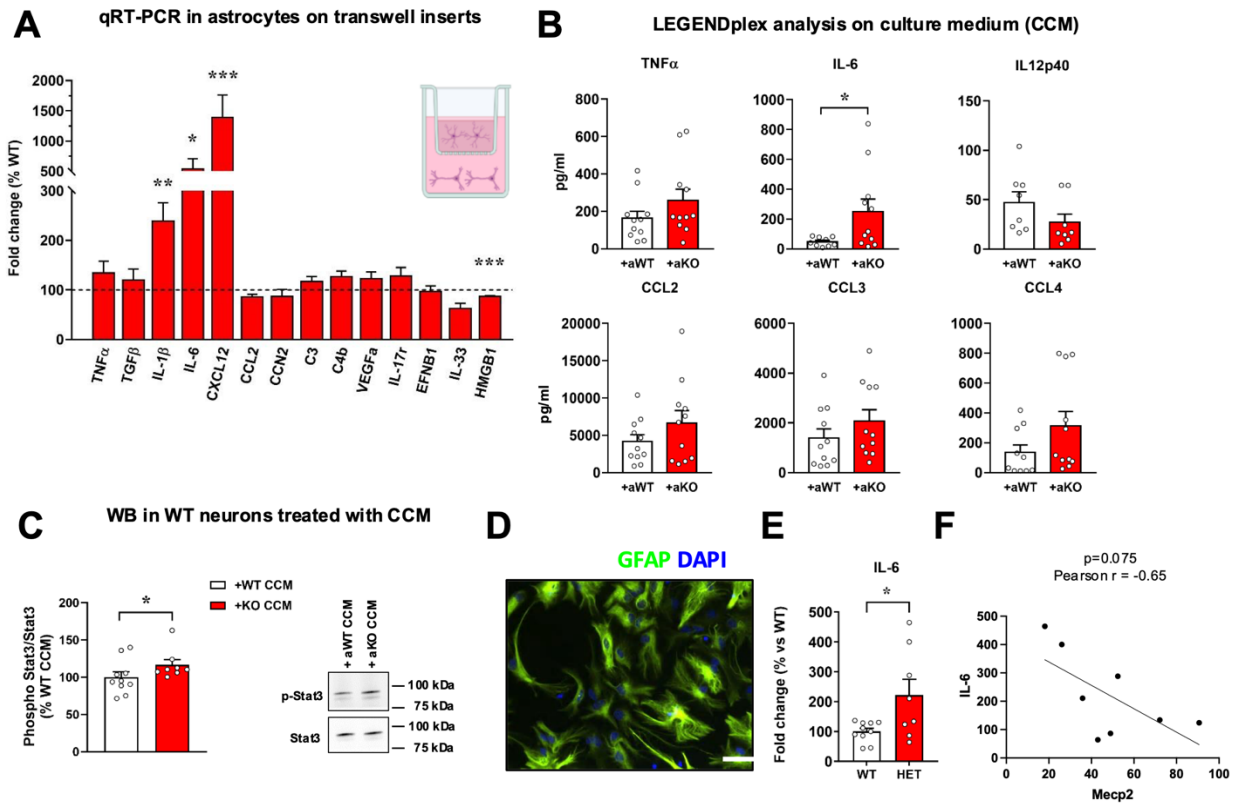

Figure 11. Mecp2 KO astrocytes secrete an excessive amount of IL-6. **(A)** mRNA levels of inflammation-related target genes in KO astrocytes cultured on transwell inserts, expressed as fold change with respect to WT astrocytes (represented by dotted line, set at 100%). **(B)** Graphs represent the amount of different cytokines detected in +aWT and +aKO CCM expressed in pg/mL. **(C)** On the left, expression level of pStat3 normalized on Stat3 in neurons treated with +aWT (set at 100%) or +aKO CCM. On the right, representative bands for pStat3 and Stat3 in western blot. **(D)** Representative image of cultured MACS-sorted astrocytes stained for GFAP. Scale bar = 30 µm. **(E)** Graph shows the level of *IL-6* mRNA expression in WT (set at 100%) and HET MACS-sorted astrocytes. Data in all the previous graphs are expressed as mean ± SEM and statistical analyses is performed by unpaired Student's t-test or Mann Whitney test according to data distribution (*p<0.05, **p<0.01, ***p<0.001). Samples derived from at least 2 independent experiments. **(F)** Correlation between *Mecp2* and *IL-6* mRNA levels in HET astrocytes isolated by MACS technology. Statistical analysis is performed by Pearson's correlation test (p=0.075) and r value indicates an indirect correlation between the expression of the two genes (r = -0.65).

4.2.3 *Mecp2* KO astrocytes secrete increased levels of IL-6 only in the presence of WT neurons

Considering that astrocyte transcriptome is strongly influenced by neuronal inputs (109), we found it interesting to determine whether the inflammatory phenotype arising

in KO astrocytes could be induced by the presence of neurons or simply derives from the absence of *Mecp2*. To answer to this question, we investigated the expression of the same set of inflammation-related genes coding from cytokines and chemokines in WT and *Mecp2* KO astrocytes cultured alone. Curiously, *IL-1β*, *IL-6* and *Cxcl12* genes, significantly upregulated in KO astrocytes cultured with neurons, are not overexpressed in KO astrocytes cultured alone. On the contrary, *Hmgb1* mRNA level remains significantly decreased also in astrocyte mono-cultures, while we found a significant downregulation in the expression of other inflammatory genes, namely *IL17R*, *Efnb1* and *Vegfa* (Figure 12A). These data demonstrate that the increased expression of specific cytokines, including IL-6, is related to the presence of neurons, revealing a non-cell autonomous mechanism triggered by the co-culture condition. To further confirm this evidence, the phosphorylation level of Stat3 is not increased when neurons are treated with the KO ACM, thus demonstrating the absence of excessive IL-6 secretion in KO mono-cultures (Figure 12B). To prove the strict dependence of IL-6 production from the presence of neuronal inputs, we measured by ELISA assay IL-6 concentration in culture medium upon neuron removal. In particular we set up the following experiment: WT neurons and KO astrocytes are cultured for 14 days, then KO astrocytes on transwell inserts are transferred in a new plate in the absence of neurons, but in the presence of the co-culture medium (CCM). ELISA assay was performed on CCM to quantify IL-6 at different time points, corresponding to the last day of co-culture, 4 and 8 days after neuron removal. After 14 days of co-culture the highest levels of the cytokine are recorded, but its amount progressively decreases until, after 8 days, it reaches the values detected in the medium of mono-cultures of KO astrocytes. This experiment demonstrates that IL-6 release progressively drops in the absence of neurons and shows how the excessive release of the cytokine from KO astrocytes is exclusively triggered by the presence of neuronal signaling (Figure 12C). Finally, we decided to investigate the influence of neuronal genotype on the expression of IL-6, including in the experimental setting the co-culture conditions between astrocytes and KO neurons. Interestingly, qRT-PCR analysis in astrocytes indicated that *IL-6* mRNA is increased in KO astrocytes only when they are exposed to WT neurons, demonstrating the impact of the genotype on the secretome of both interacting cell types. Therefore, this evidence further highlights the complexity of the interactions occurring between cells with different genotypic background in HET RTT brains (Figure 12D).

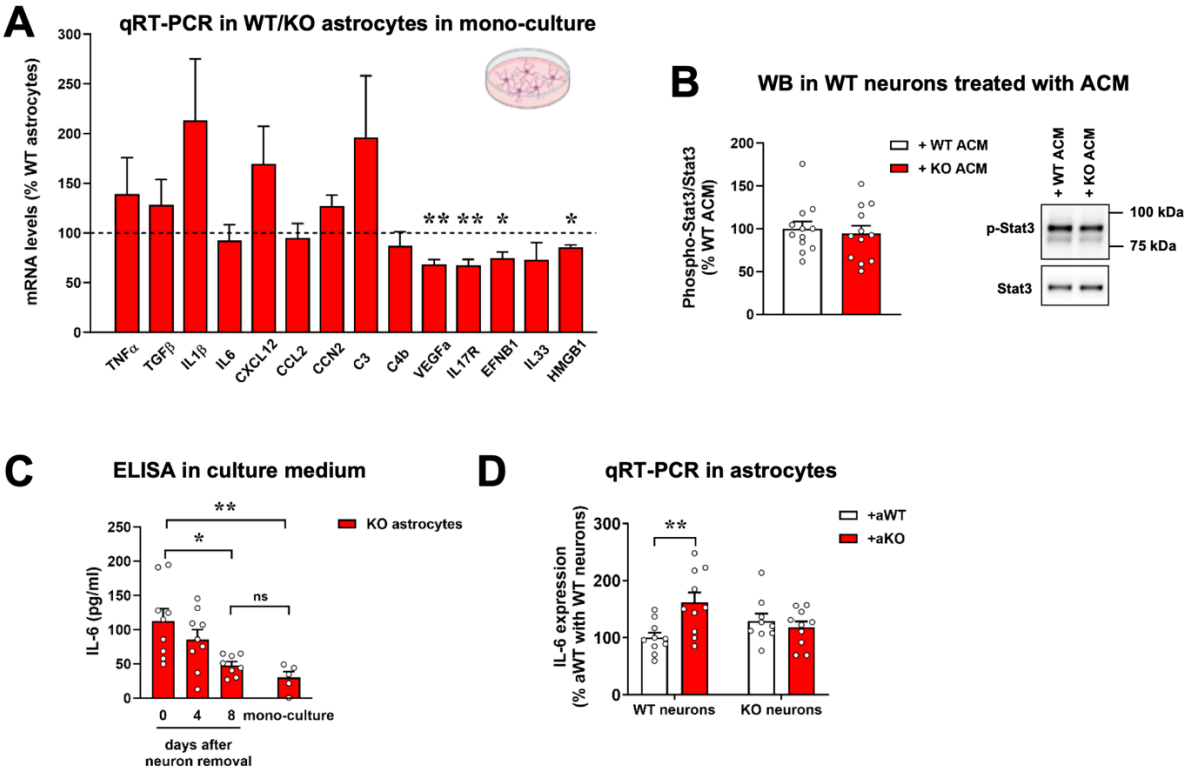

Figure 12. Mecp2* KO *astrocytes secrete an excessive amount of IL-6 only when cultured with WT neurons. **(A)** mRNA levels of inflammation-related target genes in KO astrocytes cultured alone, expressed as fold change with respect to WT astrocytes in mono-culture (represented by dotted line, set at 100%) (n=10). **(B)** On the left, expression level of pStat3 normalized on Stat3 in neurons treated with either WT ACM (set at 100%) or KO ACM. On the right, representative bands for pStat3 and Stat3 in western blot. Data in these graphs are represented as mean ± SEM. Statistics is performed by Student's t test or Mann-Whitney test in accordance with data distribution (*p<0.05, **p<0.01). **(C)** Graph shows the quantification of IL-6 concentration expressed in pg/mL in +aKO CM after the removal of neurons at different time points. As control, analysis was also performed in KO ACM. Data are represented as mean ± SEM. Statistic is done by one-way ANOVA test, followed by Kruskal-Wallis test (*p<0.05. **p<0.01). **(D)** mRNA levels of *IL-6* in astrocytes from 4 different experimental conditions (WT and KO astrocytes cultured with either WT or KO neurons). Data are represented as mean ± SEM and statistic is performed by two-way ANOVA test, followed by Tukey's post hoc test (**p<0.01).

4.2.4 Secreted IL-6 contributes to the impairment of synaptic phenotype in WT neurons

To assess the contribution of secreted IL-6 in the occurrence of neuronal defects induced by KO astrocytes, we decided to prevent its activity by adding a neutralizing antibody (anti-IL-6) in the co-cultures (Figure 13A). Fist, we assessed the efficacy of the antibody in sequestering and preventing the action of IL-6 by western blot analysis, evaluating the phosphorylation level of Stat3 in neurons co-cultured KO astrocytes. We found that the treatment with the anti-IL-6 antibody at DIV5 and DIV12 was sufficient to diminish Stat3 phosphorylation in +aKO cultures (Figure 13B).

Thus, we started investigating the effect of IL-6 inhibition on neuronal morphology, which has been extensively reported to be impaired in neurons cultured with RTT astrocytes (103,151). For this purpose, we measured dendritic length of neurons cultured for 6 days with either WT or KO astrocytes in presence or absence of anti-IL-6 (added at DIV5). Neurons were fixed and stained for the cytoskeletal marker MAP2 to highlight dendrites and NeuronJ was used to measure total dendritic length. Our data confirmed that the presence of KO astrocytes causes a significant reduction of dendritic length, that, interestingly, is fully rescued by IL-6 blockade (Figure 13C-13D). Having already proved that KO astrocytes are not able to correctly sustain synapse formation and maturation, we also tested the involvement of IL-6 in the reported synaptic defects. Indeed, we performed immunofluorescence staining of Synapsin1/2 and Shank2 synaptic proteins in the same co-culture conditions, treating +aWT and +aKO cultures with IL-6 neutralizing antibody at DIV5 and DIV12 (Figure 13E-13H). Our results showed that sequestering IL-6 prevents the synaptotoxicity induced by KO astrocytes, eliciting a complete rescue of the level of Synapsin1/2 together with a significant amelioration of the colocalization of the two synaptic proteins. Importantly, the same treatment did not provide a complete rescue of Shank2 puncta density, suggesting that other factors, beyond IL-6, are contributing to the synaptic defects induced by RTT astrocytes. In addition, we highlighted that blocking the activity of this cytokine on neurons co-cultured with WT astrocytes (+aWT) caused a slight detrimental effect, thus confirming the crucial role of IL-6 in physiological conditions (171). To verify that the beneficial effect of the treatment observed on +aKO neurons was specifically related to the administration of the neutralizing antibody, we also treated co-cultures with an isotypic antibody (Rat

IgG) following the same protocol. As expected, this IgG treatment was not effective and the pre- and post-synaptic defects persisted in neurons exposed to KO astrocytes (Figure 13E-13H).

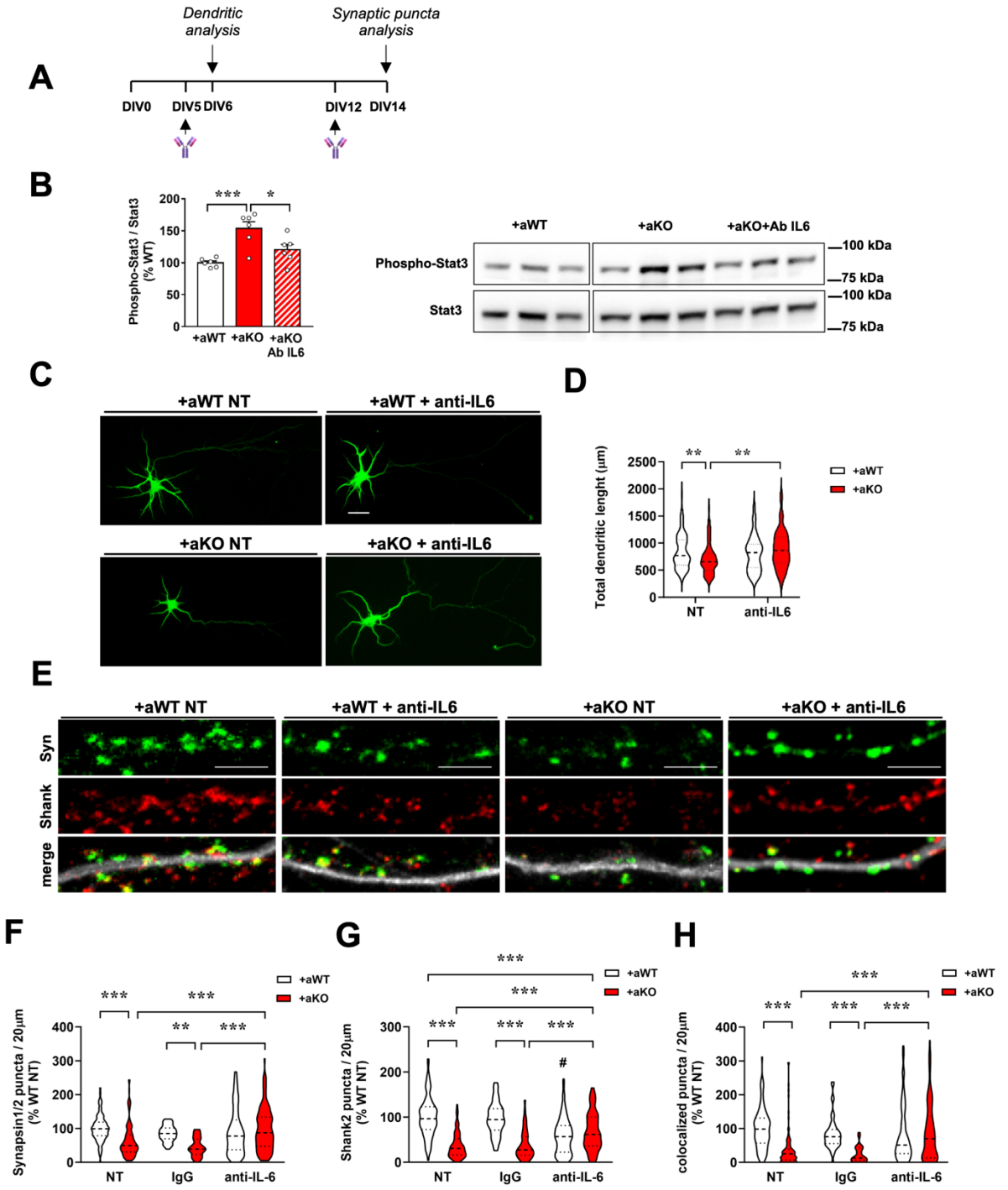

Figure 13. Treatment with a neutralizing antibody for IL-6 ameliorates neuronal defects. **(A)** Experimental setting of anti-IL-6 (or isotypic antibody) treatment in transwell-based co-culture system. Neutralizing antibody is added at DIV5 and DIV12 for immunofluorescence analysis on DIV14 neurons, while is only administered at DIV5 for morphological analysis performed on DIV6 neurons. **(B)** Graph shows the level of phosphorylated Stat3 (pStat3)

normalized on total Stat3 content of +aWT and +aKO neurons with or without neutralizing antibody. Data are expressed as mean ± SEM and statistical analysis is performed by one-way ANOVA followed by Tukey's post hoc test (*p<0.05, ***p<0.001). On the right, representative western blot bands of pStat3 and Stat3. **(C)** Representative images of immunofluorescence staining for the dendritic marker MAP2 of +aWT and +aKO neurons treated with neutralizing antibody or left untreated (NT). Scale bar = 20 μm. **(D)** Total dendritic length (μm) analysis of +aWT and +aKO treated and untreated neurons is represented by violin plot. The analysis was performed on n>40 neurons per experimental group from 5 biological replicates. Statistical analysis is performed by two-way ANOVA test, followed by Tukey's post-hoc test (**p<0.01). **(E)** Representative images of primary branches acquired from +aKO and +aWT neurons treated with neutralizing antibody, IgG or left untreated (NT) stained for Synapsin1/2 (green), Shank2 (red) and their merge with MAP2 (white). Scale bar = 5 μm. **(F-H)** Violin plots depicts the median (dashed line) and 25th and 75th percentiles (dotted lines) of the puncta density of Synapsin1/2 **(F)**, Shank2 **(G)** and the level of their colocalization **(H)** +aKO and +aWT neurons treated with neutralizing antibody, IgG or left untreated (NT). Data are expressed as mean ± SEM and statistical analysis is performed by two-way ANOVA followed by Tukey's post-hoc test (**p<0.01, ***p<0.001). #p<0.0001 indicates the comparison between +aWT treated with neutralizing antibody versus NT or IgG treated +aWT neurons. Data are collected from n>4 biological replicated with more than 50 neurons analyzed for each experimental group.

Given that many factors secreted by astrocytes likely contribute to the neuronal defects observed in RTT, we aimed at evaluating the contribution of exclusively IL-6 to the synaptic phenotype reported in +aKO co-cultures. Therefore, we treated WT neuron with recombinant IL-6 at the dosage deduced from LEGENDplex analysis (200 pg/mL) administered every two days starting from DIV2 until DIV14. This treatment was sufficient to reduce the number of Synapsin1/2 puncta and to cause a slight decrease of post-synaptic marker Shank2. Moreover, IL-6 treatment elicited a detrimental effect on the colocalization of pre- and post-synaptic markers, thus reducing the number of active synapses (Figure 14). This experiment further underlines the toxic effect of the reported dosage of the cytokine, while confirming the involvement of other factors in the detrimental effect observed on post-synaptic phenotype.

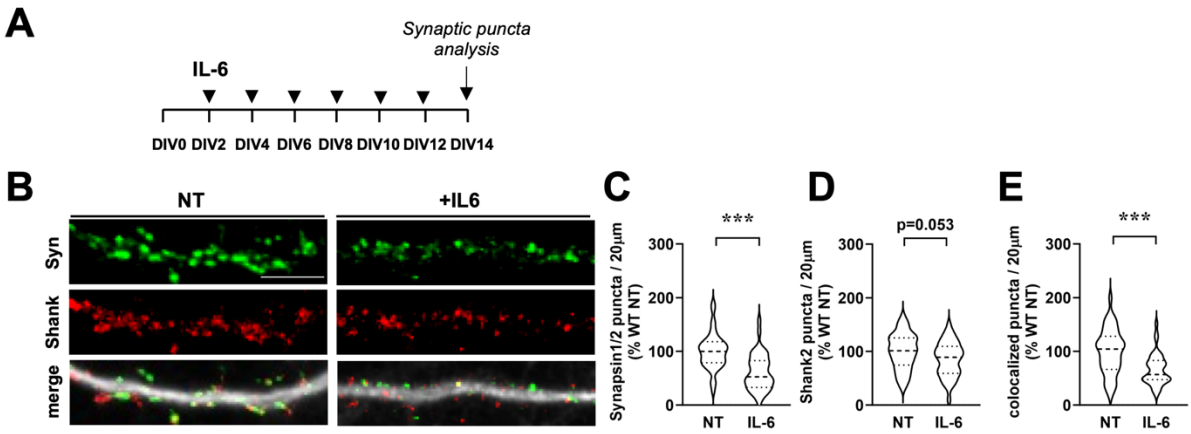

Figure 14. Recombinant IL-6 administration is synaptotoxic for WT neurons. **(A)** Experimental setting of recombinant IL-6 treatment (200 pg/mL) performed on WT neurons every two days until DIV14 when immunofluorescence staining for synaptic puncta is performed. **(B)** Representative images of primary dendrites from WT neurons left untreated (NT) or treated with IL-6, and stained for Synapsin1/2 (green) and Shank2 (red) and MAP2 (white in the merge image). **(C-E)** Violin plots show the median (dashed line) and 25th and 75th percentiles of Synapsin1/2 **(C)** and Shank2 **(D)** puncta density in 20 µm and their colocalization **(E)** in NT and IL-6 treated neurons. Data are indicated as mean ± SEM and statistic is performed by unpaired Student's t-test (***p<0.001). Analyses were performed on n>40 neurons deriving from 4 biological replicates for each experimental group.

4.3 IL-6 expression shows a trend toward an increase in the whole cortex of symptomatic HET mice

After assessing the increased levels of IL-6 *in vitro* by *Mecp2* KO cortical astrocytes in the transwell-based system and *in vivo* by astrocytes sorted from the cortex of young (P7) HET mice, we started characterizing its expression in symptomatic mice. Our major aim is to describe the temporal expression of the cytokine and its downstream pathway in RTT brain to establish its correlation with RTT progression, and, as a logic consequence, to investigate whether its blockade could alleviate synaptic defects also *in vivo* and improve neurological alterations.

In details, by qRT-PCR, we assessed the level of *IL-6* and *Stat3* mRNA in P100 and P200/250 HET animals, both in the cortex (CTX) and hippocampus (HP), two of the main affected brain areas in RTT (11, 21–23). We found a tendency to the increment of IL-6 in HET cortices at both time points (14A and 14C), without observing any

difference in hippocampus (Figure 14F and 14H). Interestingly, Pearson's correlation test revealed a tendency toward a direct correlation between the levels of *IL-6* and *Stat3* in HET samples, highlighting that, even in a more complex model comprising many different cell types carrying a different genetic background, the expression of *IL-6* is actively triggering the activation of its downstream pathway (Figure 14E). Therefore, to further investigate IL-6 signaling, we analyzed the transcriptional and protein expression of Stat3, as well as its phosphorylation in both cerebral regions. Overall, data indicate that the Stat3 phosphorylation does not change between the experimental groups (Figure 15B, 15D, 15G and 15I), while we reported an increased protein expression of Stat3 protein in P200/P250 HET cortex and a tendency towards the increase of Stat3 mRNA level at P100 (Figure 15D). These slight alterations might depend on the selective deregulation of IL-6 in astrocytes, thus the analysis in the whole cortex and hippocampus could dilute the defects. For this reason, in the next future, we aim at directly analyzing the protein levels of the cytokine in astrocytes sorted from WT and symptomatic HET mice cortices at P100.

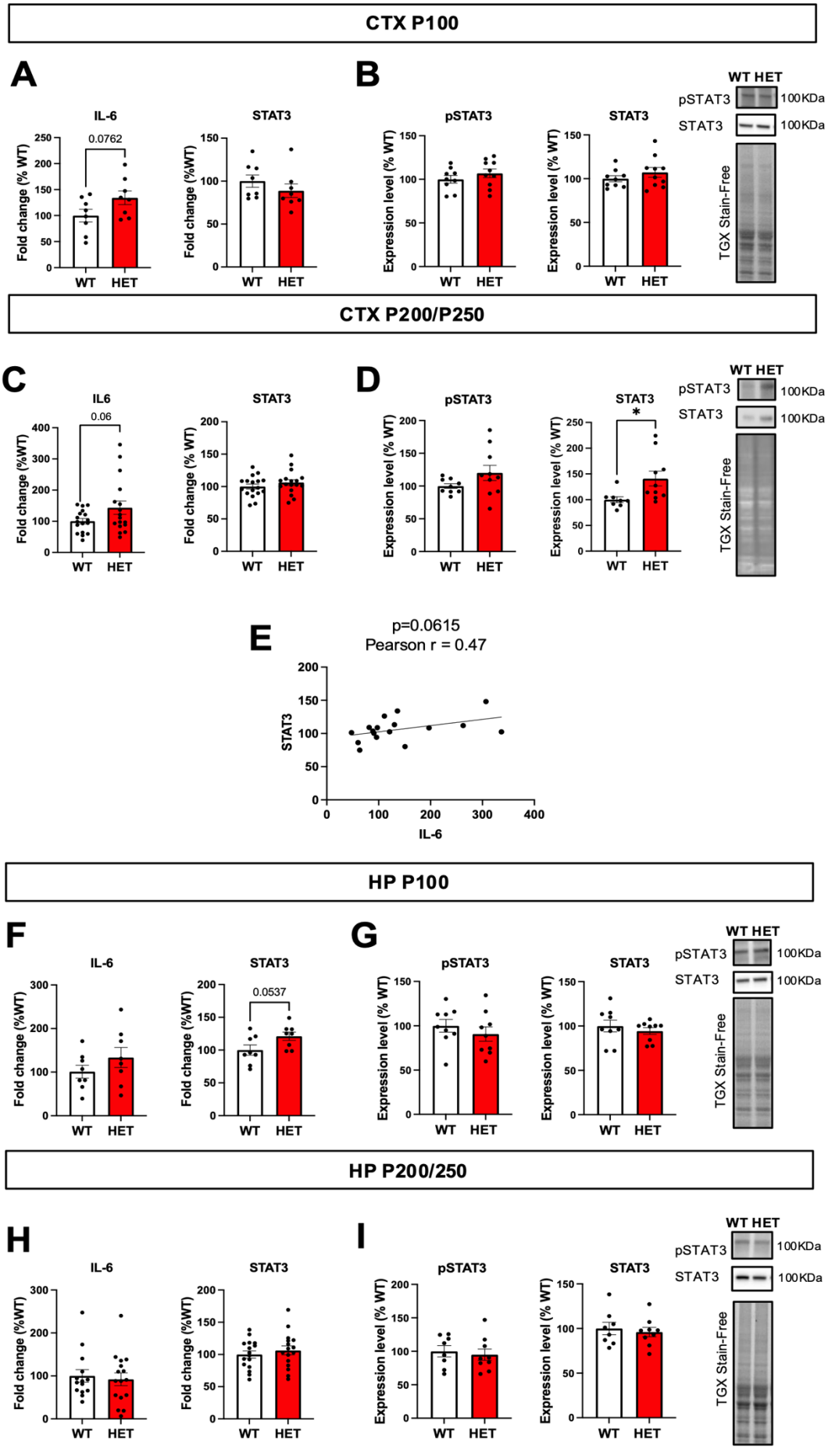
CTX P100
A
IL-6
0.0762
Fold change (% WT)
WT
HET
STAT3
Fold change (%WT)
B
pSTAT3
Expression level (% WT)
STAT3
WT HET
pSTAT3
100KDa
STAT3
100KDa
TGX Stain-Free
CTX P200/P250
C
IL6
0.06
Fold change (%WT)
STAT3
D
pSTAT3
STAT3
*
E
p=0.0615
Pearson r = 0.47
STAT3
IL-6
HP P100
F
IL-6
STAT3
0.0537
G
pSTAT3
STAT3
HP P200/250
H
IL-6
STAT3
I
pSTAT3
STAT3